CDF/ANAL/BOTTOM/CDFR/9743
Version 4.0
April 29, 2009

# Study of the $B_s^0 \to \phi\phi$ decay and measurement of its Branching Ratio

**Authors:** B. Di Ruzza[1], L. Ortolan[2],
Giacomo Artoni, Marco Rescigno, A.M. Zanetti

**Abstract**

We present a study of the $B_s^0 \to \phi\phi$ decay in the Two Track Trigger sample with $2.9 fb^{-1}$ of data collected up to April 2008. Signal yields of the $B_s^0 \to \phi\phi$ and the $B_s^0 \to J/\psi\phi$ decays are presented; the $B_s^0 \to J/\psi\phi$ is used as a normalization channel in the measurement of the Branching Ratio ($BR$) of $B_s^0 \to \phi\phi$. The trigger and selection efficiencies and the muon efficiency are evaluated. The ratio of the $BR(B_s^0 \to \phi\phi)$ to the $BR(B_s^0 \to J/\psi\phi)$ is measured as $R = BR(B_s^0 \to \phi\phi)/BR(B_s^0 \to J/\psi\phi) = [174 \pm 11(stat) \pm 22(syst)] \cdot 10^{-4}$ and is used to compute the Braching Ratio of $B_s^0 \to \phi\phi$, $BR(B_s \to \phi\phi) = []2.35 \pm 0.15(stat) \pm 0.29(syst) \pm 0.80(BR) \cdot 10^{-5}$. An improvement of a factor 5 on the statistical error compared to the previous measurement is achieved.

[1]diruzza@fnal.gov
[2]loreorto@fnal.gov

# Contents


1 Introduction 3

2 Datasets and Reconstruction tools 3
2.0.1 Candidate preselection . . . . . 4

3 Montecarlo Data and its Validation 4
3.1 The Monte Carlo validation . . . . . 5

4 Optimization Procedure for $B_s^0 \to \phi\phi$ Signal 11

5 Optimization Procedure for $B_s^0 \to J/\psi\phi$ Signal 16

6 Measurement of the Signal Yields 19
6.1 $B_s \to J/\psi\phi$ events . . . . . 19
6.1.1 The signal . . . . . 19
6.1.2 The combinatoric background . . . . . 21
6.1.3 The reflections . . . . . 21
6.1.4 Final fit . . . . . 23
6.2 $B_s \to \phi\phi$ events . . . . . 24
6.2.1 The signal . . . . . 24
6.2.2 The combinatoric background . . . . . 26
6.2.3 The reflections . . . . . 26
6.2.4 Final fit . . . . . 27

7 Measurement of $BR(B_s^0 \to \phi\phi)$ 28

8 Trigger and Selection Efficiencies 29

9 Muon Efficiency 31
9.1 Efficiency of requiring the $HasMuon$ flag . . . . . 32
9.2 Muon Efficiency vs $\phi$ and $\eta$ . . . . . 35
9.3 Total Muon Efficiency . . . . . 36
9.4 Systematic Uncertainty on Muon Efficiency . . . . . 38

10 Systematic Uncertainties 39
10.1 Systematic uncertainty on the number of events . . . . . 40
10.1.1 Fit range . . . . . 40
10.1.2 Signal parametrization . . . . . 41
10.1.3 Total uncertainties . . . . . 41
10.2 Uncertainties on the background subtraction . . . . . 41
10.3 $\eta$ dependence of $\varepsilon_\mu$ . . . . . 41
10.4 Uncertainty on the trigger and selection efficiencies ratios . . . . . 42
10.4.1 Polarization and lifetime values in Monte Carlo . . . . . 42

10.4.2 Particle dependent XFT efficiency . . . . . . . . . . . . . . . . . . 42
10.5 Errors on Branching Ratios . . . . . . . . . . . . . . . . . . . . . . . . 43
10.6 Summary . . . . . . . . . . . . . . . . . . . . . . . . . . . . . . . . . . 44

**11 Results 45**

**12 Outlook 45**

**13 History of Changes to This Document 46**

# 1 Introduction

The $B_s^0 \to \phi\phi$ decay has been observed for the first time by CDF in 2005 [1] in a data sample of 180 $pb^{-1}$; 8 events have been seen and a first measurement of the Branching Ratio ($BR$) has been performed obtaining $BR(B_s \to \phi\phi) = [1.4 \pm 0.6(stat) \pm 0.6(syst)] \cdot 10^{-5}$. In this note we present an update of this measurement with an integrated luminosity of $2.9 fb^{-1}$ and data collected with the Two Track Trigger.

Charmless $B_s^0$ decays currently can be studied only at the Tevatron and represent a field still to be fully explored that offers additional ways to test our present theoretical understanding. The $B_s^0 \to \phi\phi$ belongs to a particular class of these decays: the $B_s$ meson decays into a pair of vector particle and the final state is self-conjugate. It can be used to measure the $B_s$ decay width difference ($\Delta\Gamma_s$), CKM studies, and tests of decay polarization predictions.

The $B_s^0 \to \phi\phi$ decay proceeds through a $b \to s\bar{s}s$ and in the Standard Model (SM) the dominant process is the $b \to s$ penguin diagram. The same penguin amplitude is involved in several processes which have shown several discrepancies with the SM predictions raising considerable attention on the theoretical side and new physics interpretations have been considered to explain the experimental data. To shed light on this experimental and theoretical rather complex scenario, new and more precise measurements are clearly needed in as many interesting channels as possible. The study of $B_s^0 \to \phi\phi$ channel is an important player in this experimental effort.

In this note we present the study of the $B_s^0 \to \phi\phi$ decay in the Two Track Trigger sample with an integrated luminosity of $2.9 fb^{-1}$. In Section 2 we present the used datasets and the main steps involved in the pre-selection of our candidates. In Sec.3 the Monte Carlo data and its validation are explained and in Sec.4 the optimization procedure used to define the analysis selection criteria both for the $B_s^0 \to \phi\phi$ and the $B_s^0 \to J/\psi\phi$ decays is presented. In Sec.6 the measurement of the signal yields of the $B_s^0 \to \phi\phi$ and $B_s^0 \to J/\psi\phi$ channels is described. The strategy employed to measure the $BR(B_s^0 \to \phi\phi)$ is illustrated in Sec.7 and the efficiencies are computed in Sec.8 and Sec.9. The systematic uncertainties are estimated in Sec.10 and the final results are shown in Sec.11.

# 2 Datasets and Reconstruction tools

The analysis described in this note uses the data sample collected with some of the trigger-paths of the Two Track Trigger (TTT). More specifically we use: `B_CHARM_LOWPT`, `B_CHARM_L1`, `B_CHARM_HIGHPT`, `B_CHARM_PHI`. Due to a wrong trigger confirmation requirement applied at the reconstruction level, the `B_CHARM_PHI` is practically totally inefficient in the current BsNtuple production and hence has not been further considered here.

The analysis is performed starting from the Bstntuples [7] available in summer 2008, i.e.:

| Period | Run Range | Location |
|---|---|---|
| 0 | 138425-186598 | bottom/hadr-80/xbhdid |
| 1-7 | 190697-212133 | bottom/bmix-60/h77jg0 |
| ”” | ”” | bottom/bmix-70/h77jm0 |
| 8-10 | 217990-233111 | bottom/hadr-80/xbhdii |
| 11-13 | 233133-246231 | cdfpbnt/xbhdij |
| 14-17 | 252836-261005 | cdfpbnt/xbhdik |

Table 1: Bstntuples used in the analysis.

These datasets correspond to a data taking period from beginning of RunII till April 2008. A goodrun list of version 23 with no requests on the calorimeter and the muon bits is used. The integrated luminosity of our sample is $2.9 fb^{-1}$.

In this note, we often refer to exclusive trigger configurations. These are defined as follow:

- HIGHPT: PrereqFast selects only `B_CHARM_HIGHPT`;
- ScA.not.HIGHPT: events selected by `B_CHARM_L1` and not by `B_CHARM_HIGHPT`;
- LOWPT.not.ScA.not.HIGHPT: events selected by `B_CHARM_LOWPT` but not by `B_CHARM_L1` and by `B_CHARM_HIGHPT`.

We request the matching between at least two reconstructed tracks and the SVT tracks. The confirmation of the `B_CHARM_LOWPT` trigger selections is imposed (trigger confirmation).

### 2.0.1 Candidate preselection

In order to obtain a smaller size Bstntuples, a skimming procedure is performed mainly aimed to reduce the combinatorial background by applying only a loose selection criteria on the B candidates. We cut on variables which should be similar in all the B decay channels under study: the decay length projected on the (x,y) plane, $L_{xy}$, and the transverse momentum, $p_T^B$, of the $B$ mesons. The cut values are:

- $L_{xy} \geq 200\mu m$
- $p_T^B \geq 5$ GeV/$c^2$

# 3 Montecarlo Data and its Validation

A simulation of the events using Monte Carlo method is required in this analysis for several reasons: the estimation of the physical background, the optimization of the cuts for the selection of the signal, the determination of trigger efficiencies for the calculation of the Branching Ratio. Thus it is important to understand when the simulation is reliable and when it is not and we perform a validation of our Monte Carlo.

We use BGenerator [8] to simulate the $b$ quark production using for $B_s^0$ spectra determined in the inclusive $H_b \to J/\psi\ + X$ cross-section measurement [9]. and their hadronization into $B$ mesons and EvtGen [10] to simulate the $B$ mesons decays.
The output of the Monte Carlo simulation is in the Bstntuple format, allowing us an easier comparison between Monte Carlo and data.

The detector and trigger configurations have undergone several variations during RunII. The simulation can access the databases and thus allows to simulate the detailed configuration of any set of real data-taking runs for modeling the realistic detector response in any given subset of data. On the other hand, the Monte Carlo is not able to reproduce exactly the trigger behavior of the trigger-paths which have a built-in dependance on the instantaneous luminosity, because this information is not stored in the database. In order to use all the trigger paths we will check that, once we re-weight Monte Carlo events in a way suitable to reproduce the different trigger mixture observed in data, a sufficiently good agreement is observed in all relevant variables.

## 3.1 The Monte Carlo validation

The validation of our Monte Carlo program consists in a test of reliability of our simulation using a comparison with the signal candidate events selected in the data. Furthermore, as explained before, in our Monte Carlo the trigger prescale cannot be simulated; so in order to make it more realistic we use a Monte Carlo with the same fractions of exclusive trigger as measured in data. In principle a single event can fire many different trigger-paths, but to re-weight the event fractions we want to use subsets of not-overlapping events.

We test the agreement of our Monte Carlo with real data comparing the distributions of several variables. The variables that are used for this purpose are the most significant for the selection and optimization procedure, such as:

- transverse momentum of the $B$ meson: $p_T^B$;
- transverse decay length of the $B$ meson: $L_{xy}$;
- impact parameter of the $B$ meson: $d_0^B$;
- impact parameter of the more energetic $\phi$: $d_{0\,max}^{\phi}$;
- transverse momentum of the $J/\psi$: $p_T^{J/\psi}$;
- transverse momentum of the less energetic kaon from $\phi$ decay: $p_T^K$;
- the bi-dimensional $\chi^2$ of the primary vertex fit: $\chi^2_{xy}$.

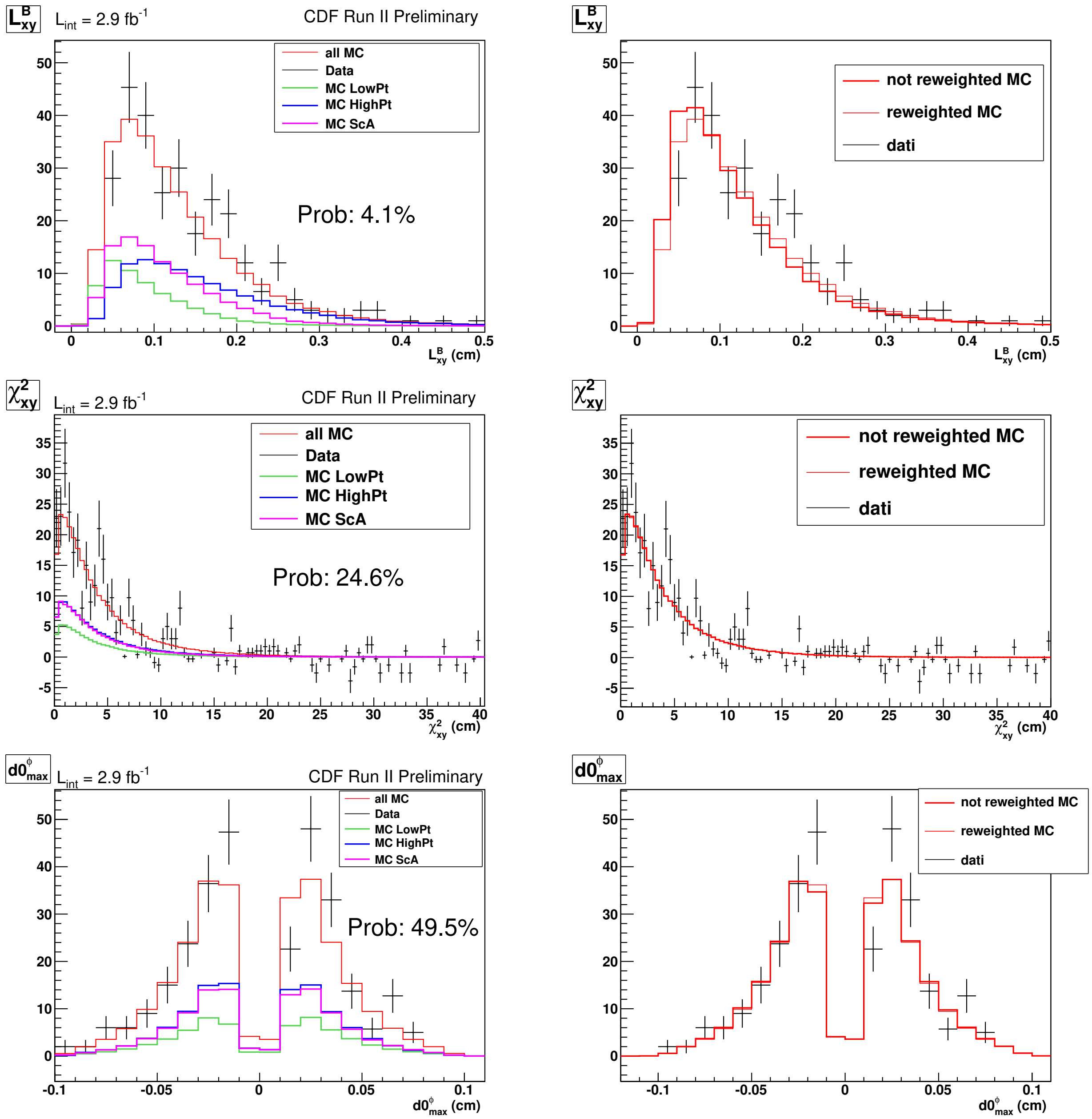


Figure 1: *Data-Monte Carlo comparison for $B_s \to \phi\phi$. On the left the data, the total MC events and divided according to different trigger-path, compared with the weighted MC; on the right comparison between weighted and not-weighted Monte Carlo events. The reported variables, from top to bottom, are: $L_{xy}$ of the $B$ meson decay, the $\chi^2_{xy}$ of the primary vertex fit, the impact parameter of $\phi$ with higher energy.*

In Figures 1 and 3 the histograms of the comparison of Monte Carlo versus data and of not-reweighted Monte Carlo versus reweighted Monte-Carlo are shown for the $B_s \to \phi\phi$ and the $B_s \to J/\psi\phi$ channels. In both cases optimized selection cuts were

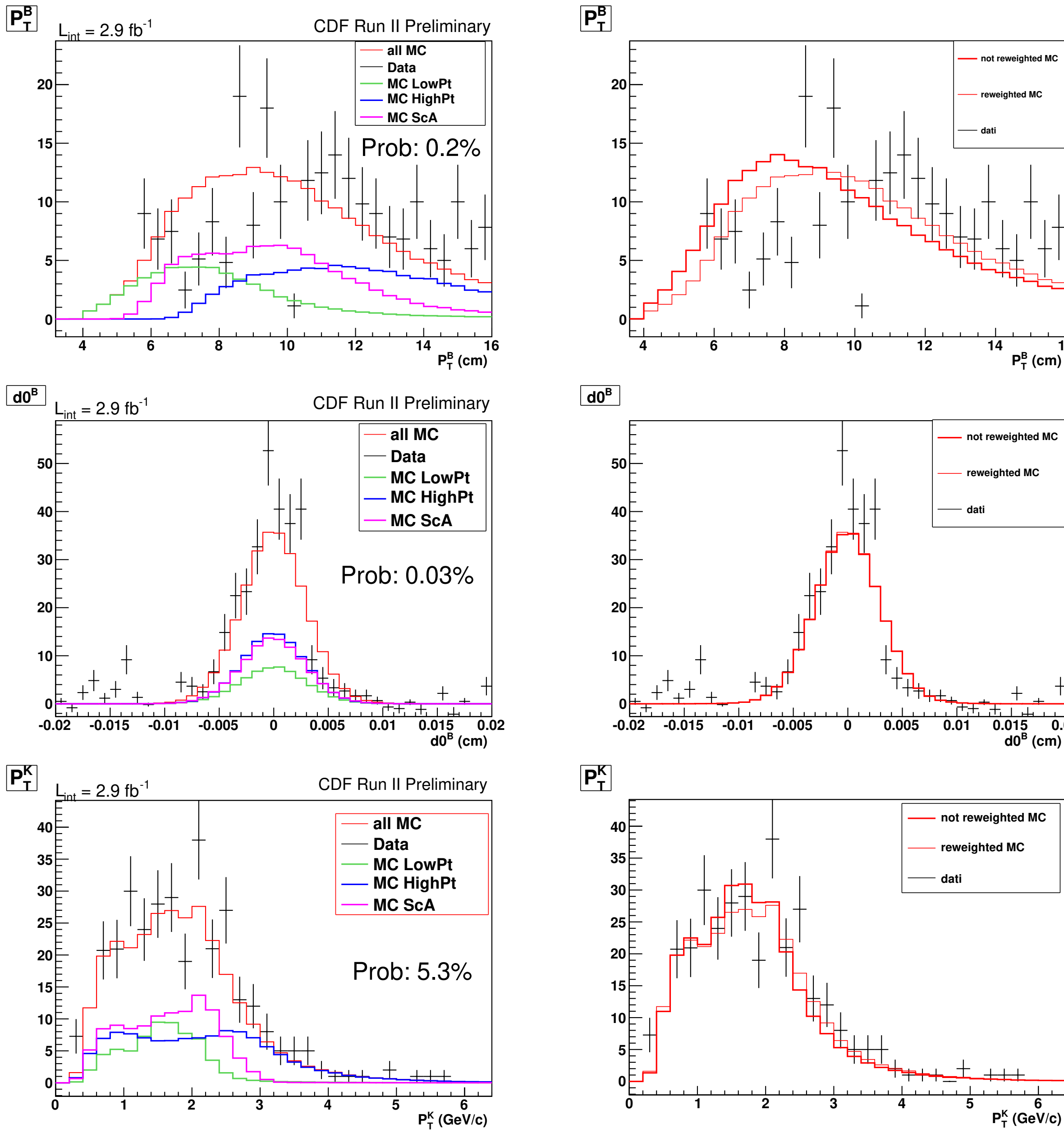


Figure 2: *As in Fig. 1 Data-Monte Carlo comparison in $B_s \to \phi\phi$ decay for B meson $p_T$, B meson impact parameter and the transverse momentum of the kaon with less energy.*

used (see section 4).
In these histograms, the background has been subtracted from the data. This subtraction (known as *sideband subtraction*) is performed subtracting from the events, in a window around the signal in the invariant mass histogram of the $B_s$ candidate, those events which are located in the same histograms in an area far from the signal peak

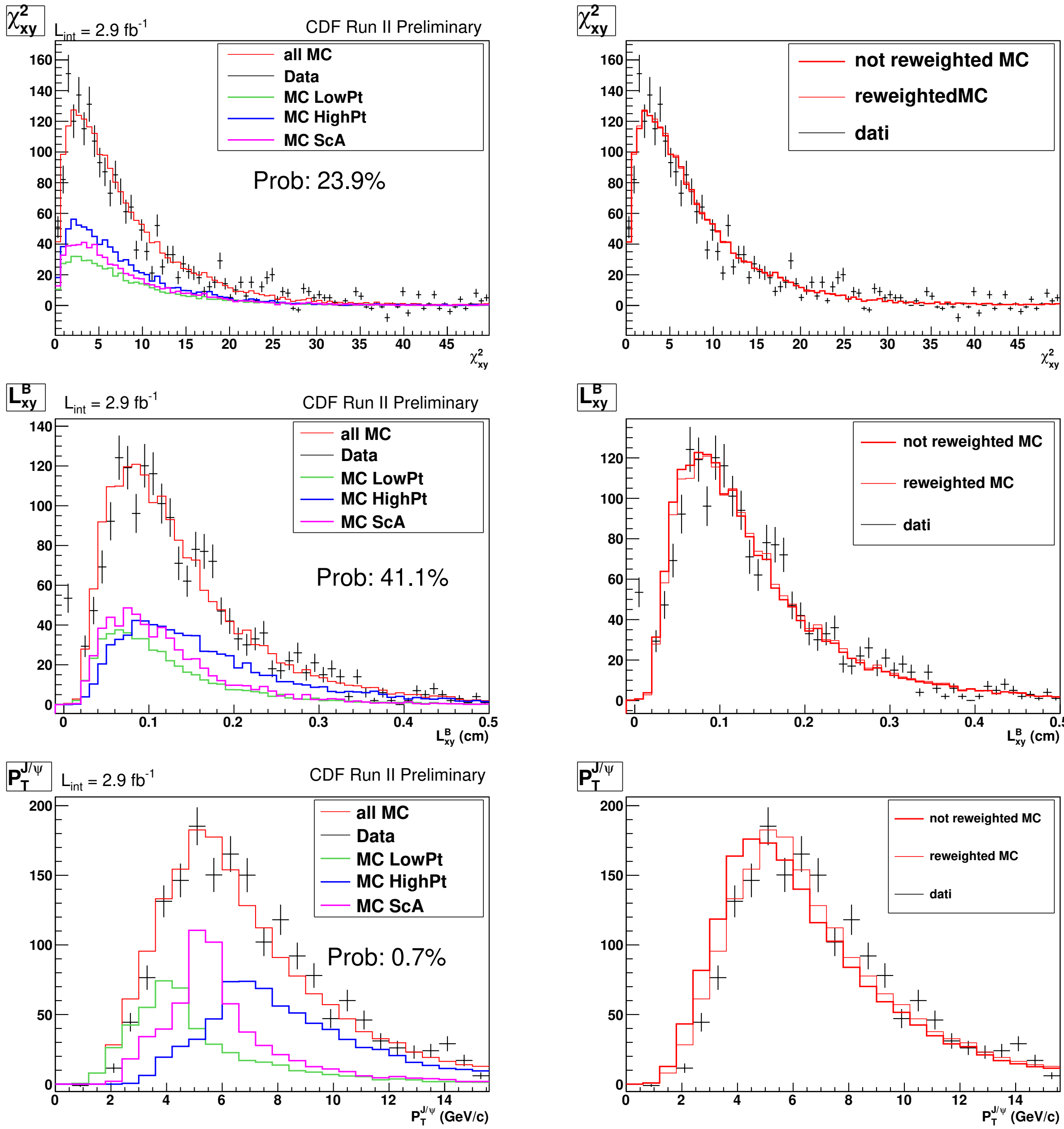


Figure 3: *Data-Monte Carlo comparison for $B_s \to J/\psi\phi$. From top to bottom the variables are: $\chi^2_{xy}$ of the primary vertex fit, the $L_{xy}$ of the $B_s$ decay, the $J/\psi$ transverse momentum.*

(sideband). We have neglected other types of background due for example to reflections of other $B$ decays. Using the Kolmogorov test we generally observe an improved agreement between data and weighted Monte Carlo histograms. Probabilities are displayed on the relevant histograms. We still observe significant disagreement only on variables directly related to the B-meson spectrum. Since this is somewhat expected, given the

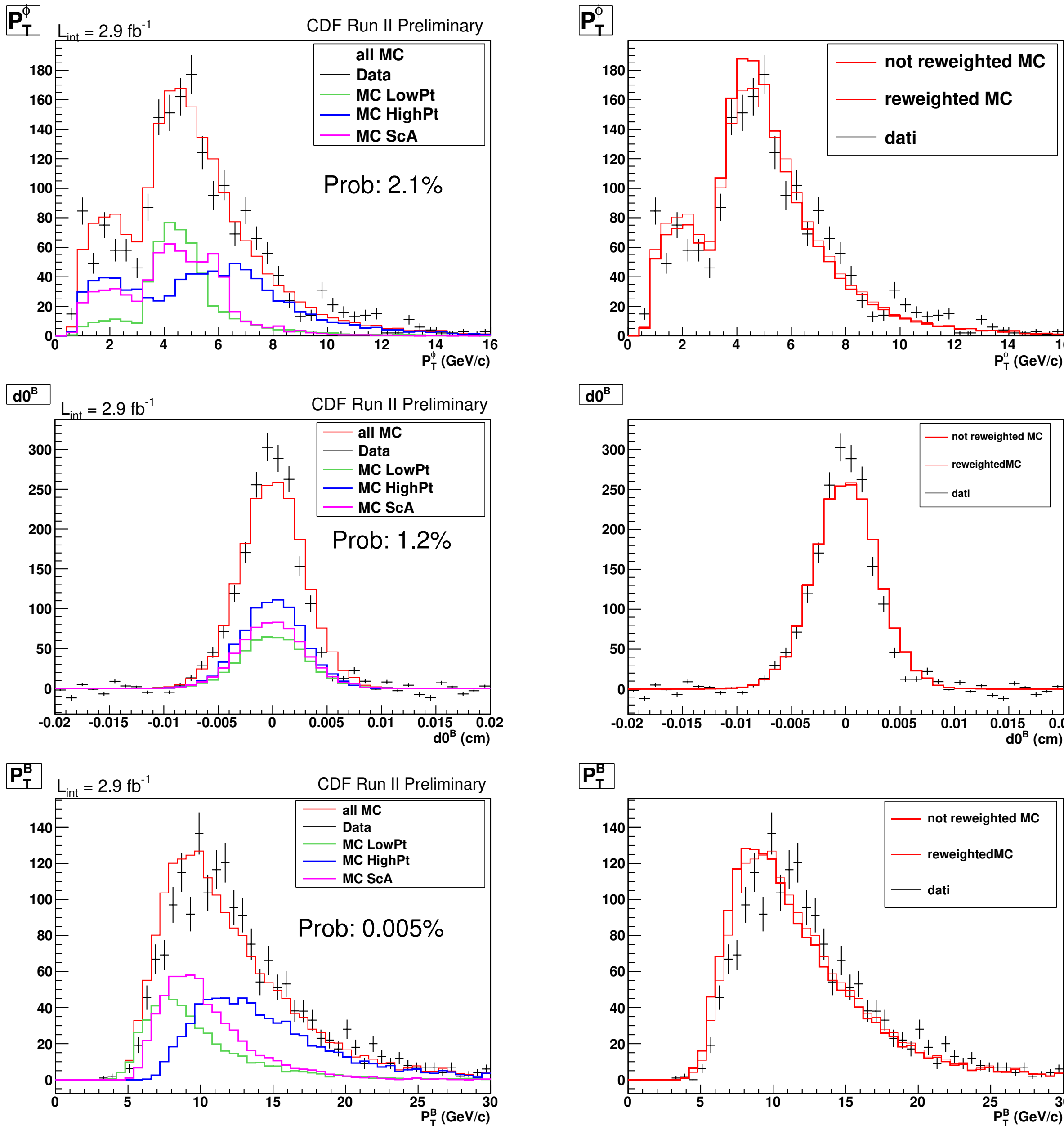


Figure 4: *As in Fig. 3 Data-Monte Carlo comparison in the $B_s \to J/\psi\phi$ decay for the $\phi$ transverse momentum and the $B_s$ meson impact parameter and $B_s$ meson transverse momentum.*

input $B_s^0$ spectrum we have used in the simulation, we will later apply a $p_T$ re-weigthing procedure to derive the efficiencies from Monte Carlo simulations. This will be based on the Data/MC comparision of $B_s^0$ $p_T$ using the large sample of $B_s^0 \to J/\psi\phi$ events. While this procedure is still to be finalized we nevertheless report in Fig. 5 the ratio of Data/MC with a preliminary fitted first-degree function overlaid. In passing we note

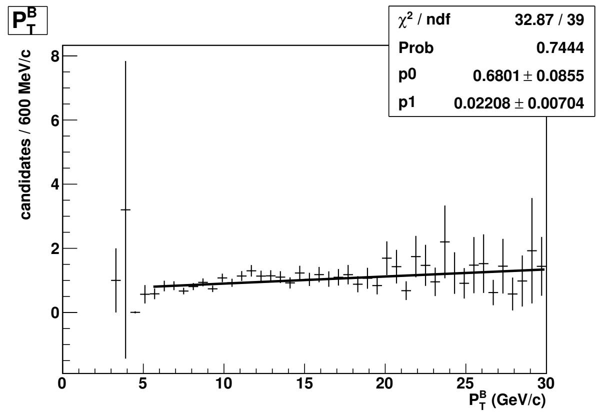


Figure 5: *Ratio of $B_s^0$ $p_T$ in Data and MC for the sideband subtracted $B_s^0 \to J/\psi\phi$ events.*

that applying this preliminary reweighting function the KS probability for the $J/\psi$ and $\phi$ $p_T$ distribution increase from 0.0067 to 0.065 and from 0.02 to 0.064 respectively.

Overall, from this study we conclude that a reasonably accurate selection of exclusive triggers in Data and Monte Carlo has been implemented, that correcting the important effect of trigger mixture produce a satisfactory simulation of typical discriminant variables and that re-wheighting the $B_s^0$ $p_T$ spectrum will likely lead to a satisfactory Monte Carlo simulation.

# 4 Optimization Procedure for $B_s^0 \to \phi\phi$ Signal

In the past [1] we had used a cut based selection aimed at maximizing the chance of either observing for the first time a $B_s^0 \to \phi\phi$ or setting a limit following the procedure of [3]. In the present circumstances we are instead interested in minimizing the statistical uncertainty in the branching ratio measurement for $B_s^0 \to \phi\phi$, thus maximising the usual figure of merit $F = \frac{S}{\sqrt{S+B}}$.

We have first to choose a set of variables in order to understand how much they can discriminate signal from background; in this particular case we used only kinematic variables, since these where the most reliable ones and they were enough to accomplish our requests. We started with those variables that had already been used in [1], that is:

- $L_{xy} \to$ distance on the $x - y$ plane between primary and secondary vertex;
- $\chi^2_{xy} \to \chi^2$ of the fit used in the reconstruction of the secondary vertex;
- $p_{t(min)} \to$ momentum of the softer $\phi$;
- $d_0 \to$ impact parameter of the reconstructed $B_S$;
- $d_{0(max)} \to$ impact parameter of the softer kaon.

Besides we decided to look for other variables that had never been used in previous analysis, such as:

- $p_{t(min)K} \to$ momentum of the softer kaon;
- $\chi^2 \to$ tridimensional $\chi^2$ of the fit in the secondary vertex reconstruction;
- $\Delta R = \sqrt{\Delta\phi^2 + \Delta\eta^2} \to$ where $\Delta\eta$ and $\Delta\phi$ stand for the difference in rapidity and azimuthal angle between the two $\phi$.

The first step towards this was to define the signal and background quantities: we estimated background in the peak region of the $B_S$ mass by defining two sidebands, one from 5.02 to 5.22 GeV/$c^2$and the other from 5.52 to 5.72 GeV/$c^2$as shown in figure 6. We then took these events and summed them to obtain an estimate of our background $B$; for what concerns signal, we used the events falling in the peak region from 5.32 to 5.42 GeV/$c^2$ $N_S$ and subtracted to these our background estimate to obtain $S = N_S - B$. In the optimization procedure we use the signal MC events normalized to the signal data events $S$ found with default cuts (as used in [1]).

Then we could look for the right variables to use and in order to do this, we produced plots 7(a), 7(b), 8(a), 8(b), 9(a), 9(b), 10(a), 10(b) with signal (blue), background (red) and MC (black) that the discrimination power for each variable and the reasonable Data/MC agreement.

At this point we were able to run our optimization, consisting in finding the set of cuts that maximises the figure of merit $F = \frac{S}{\sqrt{S+B}}$. We used five variables at a time,

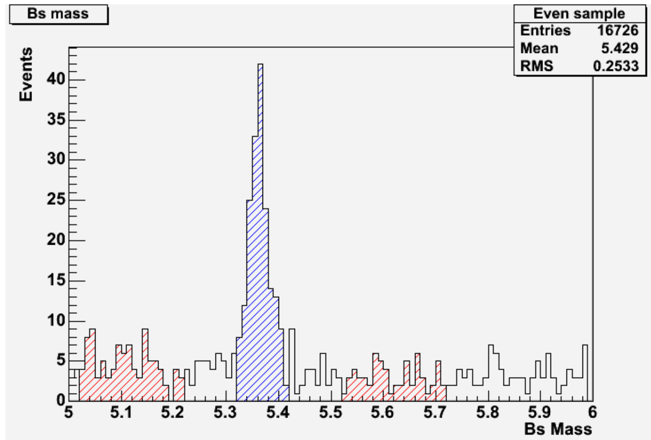


Figure 6: Massa invariante del $B_S$

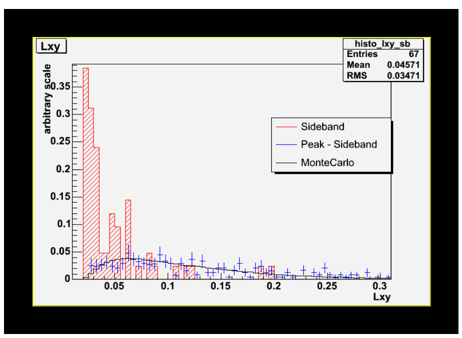


(a) $L_{xy}$

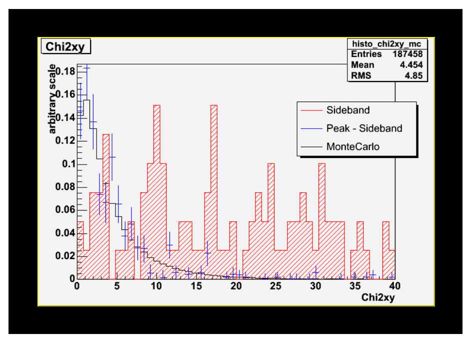


(b) $\chi^2_{xy}$

Figure 7: Signal (blue), background (red) and MC (black) distributions for $L_{xy}$ e $\chi^2_{xy}$

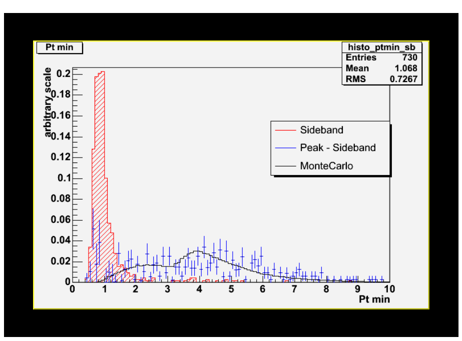


(a) $p_{t(min)}$

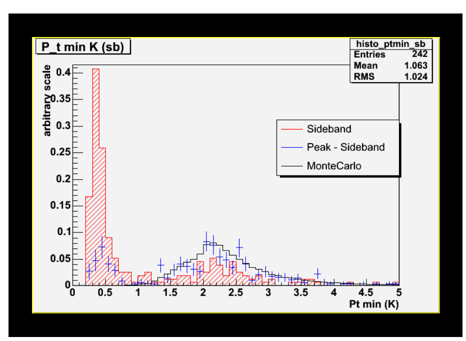


(b) $p_{t(min)K}$

Figure 8: Signal (blue), background (red) and MC (black) distributions for $p_{t(min)}$ e $p_{t(min)K}$

performing eight steps for each variable: this means that we had 32768 combinations of

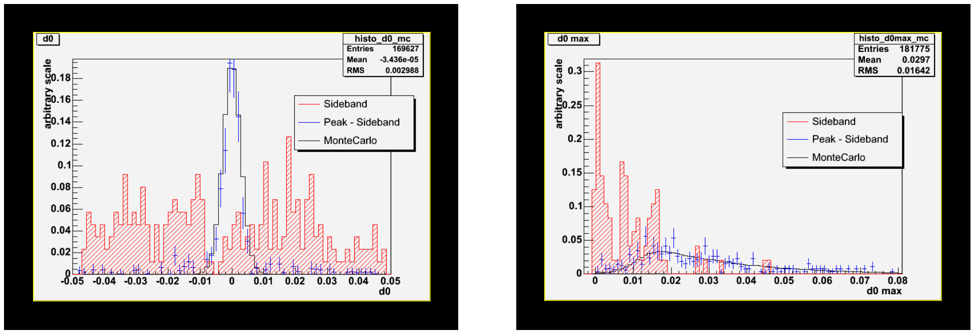


(a) $d_0$ (b) $d_{0(max)}$

Figure 9: Signal (blue), background (red) and MC (black) distributions for $d_0$ e $d_{0(max)}$

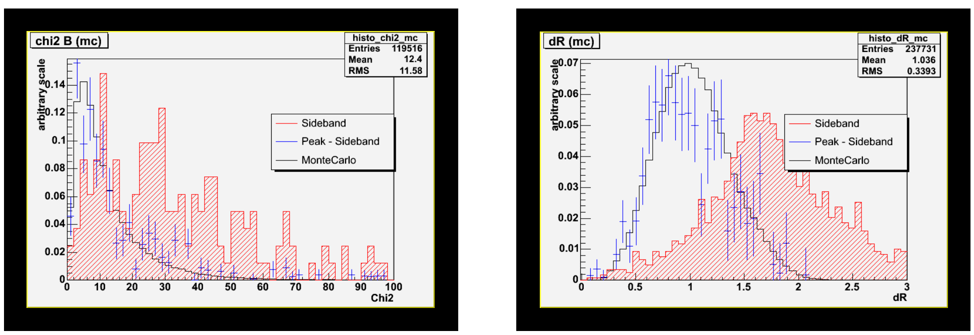


(a) $\chi^2$ (b) $\Delta R$

Figure 10: Signal (blue), background (red) and MC (black) distributions for $\chi^2$ e $\Delta R$

different cuts. In particular we performed this analysis using two different methods in order to have a cross-check and estimate the sensitivity of the optimization procedure to the detail of MC simulation:

- Standard method: our background estimate is made on data while our signal estimate is made on MC; in this case we can then use the output of our analysis without entering a bias in the process.

- MC-free method [4]: we used only the data and performing the same analysis, which means that both signal and background are obtained by the data; the problem is that we need to split our sample into two halves (randomly thus avoiding any bias) and then having the analysis performed on both of them; in this way we could use one sample to obtained the optimized cuts, and then use them on the other sample (and viceversa of course), in order to check if there were discrepancies between this two halves or between this method and the other.

Here are the results we obtained:

| Variables used | Standard method | MC-free method |
|---|---|---|
| $d_0$ $d_{0(max)}$ $L_{xy}$ $\chi^2_{xy}$ $p_{t(min)}$ | $16.8 \pm 0.5$ | $16.6 \pm 0.5$ |
| $d_0$ $\Delta R$ $L_{xy}$ $\chi^2$ $p_{t(min)K}$ | $16.5 \pm 0.5$ | $16.9 \pm 0.5$ |
| $d_0$ $d_{0(max)}$ $L_{xy}$ $\chi^2_{xy}$ $p_{t(min)K}$ | $17.2 \pm 0.6$ | $16.6 \pm 0.5$ |
| $d_0$ $d_{0(max)}$ $L_{xy}$ $\chi^2$ $p_{t(min)}$ | $16.5 \pm 0.5$ | $16.4 \pm 0.6$ |
| $d_0$ $d_{0(max)}$ $L_{xy}$ $\chi^2$ $p_{t(min)K}$ | $16.3 \pm 0.5$ | $16.7 \pm 0.5$ |

Table 2: Maximum values of $\frac{s}{\sqrt{s+b}}$ found for five combinations of variables and both methods

It is easy to notice that our results don't change that much choosing different methods or different variables. This allows us to keep on using (where it is preferable), those variables that had previously been used and that are well reproduced by MC, since $\chi^2$, $\Delta R$ and $p_{t(min)K}$ only slightly improve our analysis. To complete this analysis we have then chosen the second set of variables for the MC-free method and the third one for the Standard method, simply because this sets were those that gave us the best results. In particular we show the plots we obtained with a projection on only one variable:

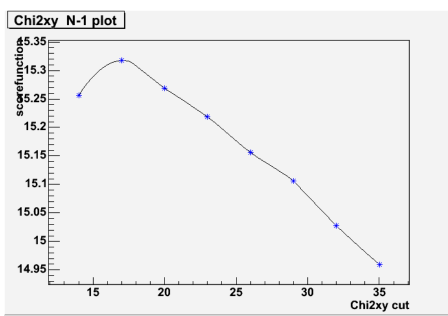


(a) $\chi^2_{xy}$

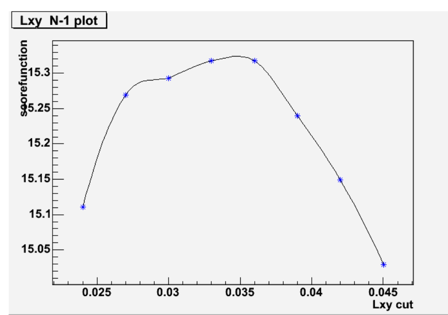


(b) $L_{xy}$

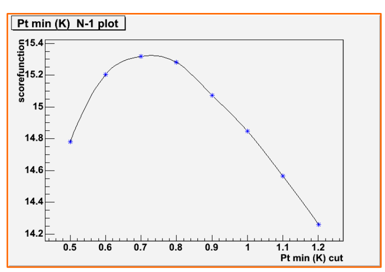


(c) $p_{t(min)K}$

Figure 11: $N-1$ plots for $\chi^2_{xy}$, $L_{xy}$ e $p_{t(min)K}$

Next table represents our optimized values for the different cuts, divided in three cases: the standard method, the MC-free method (note that there should be two values for this method, but in this particular case they were coincident), and the analysis of [1].

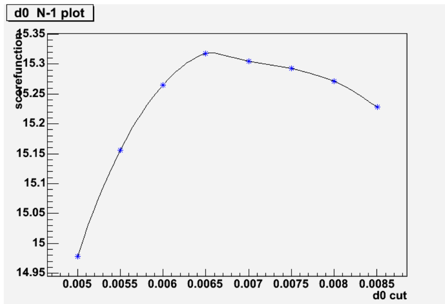


(a) $d_0$

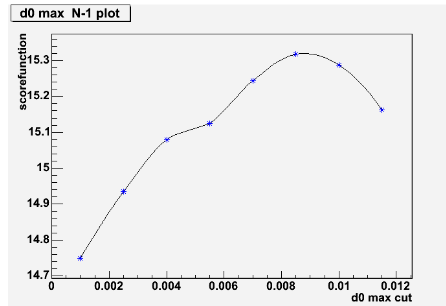


(b) $d_{0(max)}$

Figure 12: $N-1$ plots for $d_0$ e $d_{0(max)}$

| Standard method | MC-free method | Analysis in [1] |
|---|---|---|
| $L_{xy} > 330\ \mu m$ | $L_{xy} > 410\ \mu m$ | $L_{xy} > 350\ \mu m$ |
| $p_{t(min)K} > 0.7\ GeV/c$ | $p_{t(min)K} > 0.75\ GeV/c$ | $p_{t(min)} > 2.5\ GeV/c$ |
| $\chi^2_{xy} < 17$ | $\chi^2_{xy} < 25$ | $\chi^2_{xy} < 10$ |
| $d_0 < 65\ \mu m$ | $d_0 < 60\ \mu m$ | $d_0 < 80\ \mu m$ |
| $d_{0(max)} > 85\ \mu m$ | $d_{0(max)} > 60\ \mu m$ | $d_{0(max)} > 110\ \mu m$ |

Table 3: Cuts optimized by different methods

We then apply these cuts obtained from our analysis (as well as the old ones) to our sample of approximately 2.9 $fb^{-1}$ in order to understand if our analysis could give an improvement; first thing we plot the $B_S$ mass applying the different cuts: Fitting

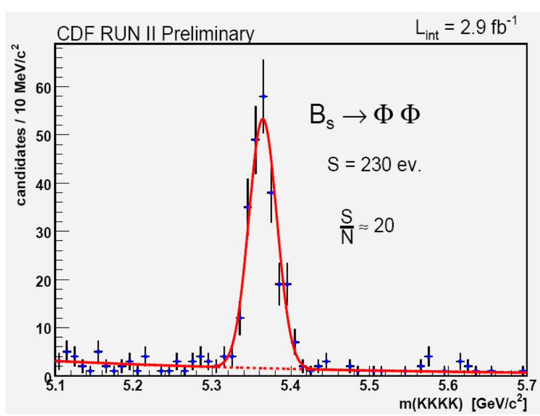


Figure 13: $B_S$ lineshape ([1])

these distributions, we check how many events we have in the peak region:

- $N_{ev} = 230 \pm 15$ for the cuts obtained with the analysis in [1];

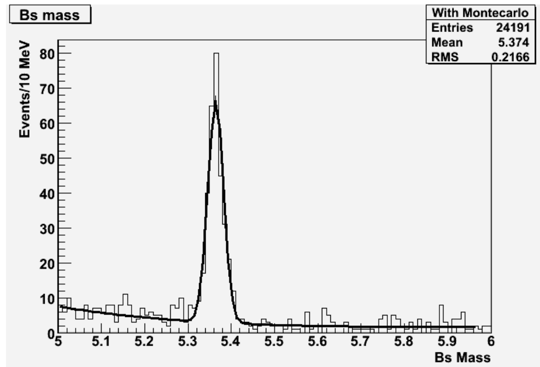


Figure 14: $B_S$ lineshape (Standard method)

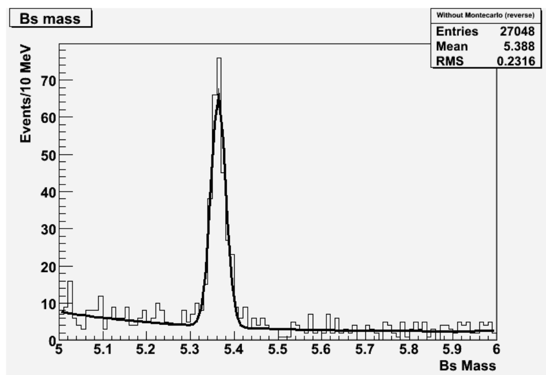


Figure 15: $B_S$ lineshape (MC-free method)

- $N_{ev} = 284 \pm 19$ for the analysis performed using MC;
- $N_{ev} = 265 \pm 18$ for the analysis that didn't rely on MC.

This means that our optimization lead to an increase of the events in the peak region of about 24%.

# 5 Optimization Procedure for $B_s^0 \to J/\psi\phi$ Signal

The cuts selection used to study this decay in the Two Track Trigger in [5] were optimized for a polarization measurement using a different score-function than $\frac{S}{\sqrt{S+B}}$. To be consistent with what we did for the signal selection for $B_s^0 \to \phi\phi$ we performed a new optimization with the standard prescription of maximizing $\frac{S}{\sqrt{S+B}}$ taking $S$ from Signal Monte Carlo normalized to observed events with cuts of [5] and $B$ from $B_s^0$ mass sidebands. We decided to use the same variables of the previous analysis because they are very similar or related to those used in $B_s \to \phi\phi$.

In Figure 16 the $N-1$ plots for the $B_s \to J/\psi\phi$ decay are shown.

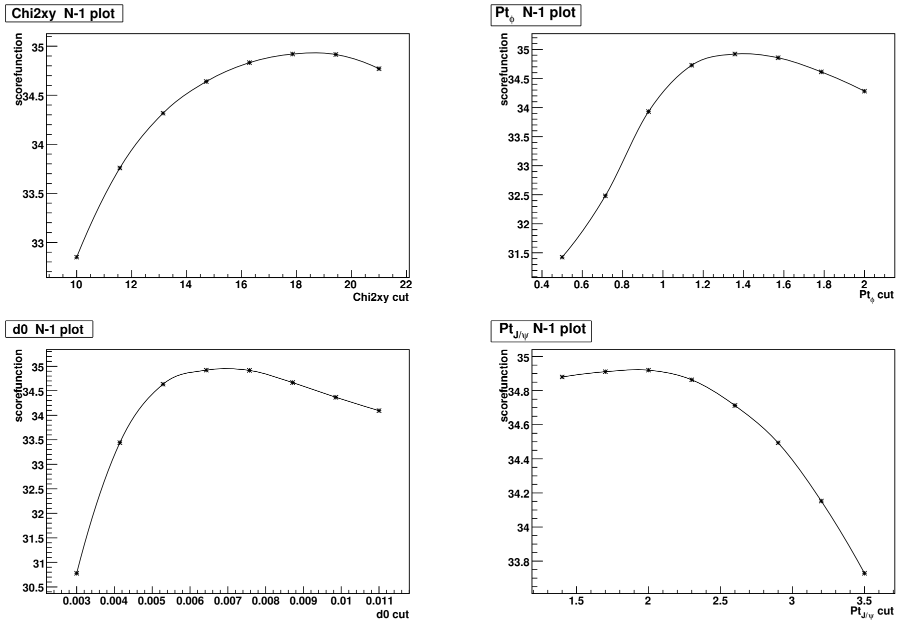


Figure 16: $N-1$ *plots of the score-functions as a function of the variable cuts for the* $B_s \to J/\psi\phi$ *decay. From top to bottom, left to right the variables are: the* $B_s$ *meson* $\chi^2_{xy}$, *the* $\phi$ *the transverse momentum, the* $B_s$ *meson impact parameter, the* $J/\psi$ *transverse momentum.*

The cut values that maximise the chosen score function are summarized in Tab.4. The optimization procedure was not as complete as the one for the $B_s \to \phi\phi$. We have not investigated, for example, other possible sets of variables. It has to be noted, however, that the impact on the Branching Ratio measurement of an even better optimization is expected to be marginal.

| Variable | Cut |
|---|---|
| $L_{xy}$ | $> 290$ $\mu$m |
| $\mathrm{P}_T^{\phi}$ | $> 1.36$ GeV/$c$ |
| $\mathrm{P}_T^{J/\psi}$ | $> 2.0$ GeV/$c$ |
| $\chi^2_{xy}$ | $< 18$ |
| $d_0{}^B$ | $< 65$ $\mu$m |
| confirmation of 1 muon | |

Table 4: *Optimal cut values for* $B_s \to J/\psi\phi$ *selection.*

The selection was optimized starting from the request of the identification of at least one muon in the $J/\psi \to \mu\mu$ decay. The choice to apply this cut allow us to obtain the best compromize about the signal-to-background ratio and to exclude the possible background arising from the $J/\psi \to ee$ decay. While a quantitative study of this component is beyond the scope of this note it is interesting to notice that requiring at least one electromagnetic object associated to the $J/\psi$ tracks a signal seems to be present (see Fig.18), although it's difficult to say because no quantitative study on background level of this selection has been made.

In Fig. 17 the effect on the $B_s^0$ mass peak of requiring 0,1 or 2 muons is shown. As expected the signal with 2 reconstructed muons is very pure, but suffer from a significant loss of efficiency.

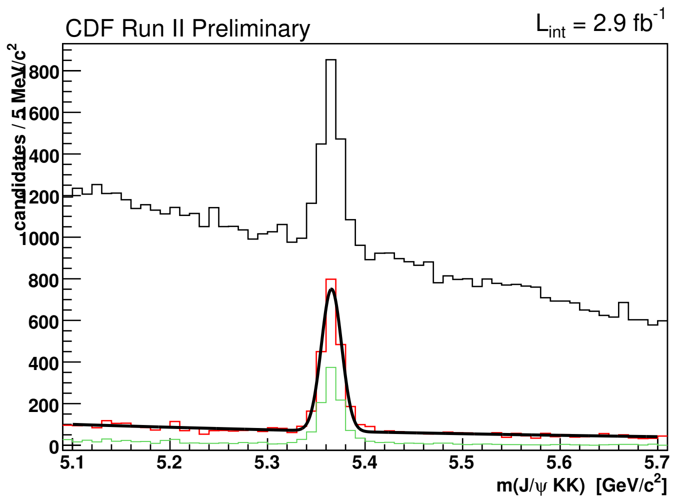


Figure 17: *Comparison of the $B_s$ invariant mass distributions obtained requiring the identification of 0 (black), 1 (red) or 2 (green) muons.*

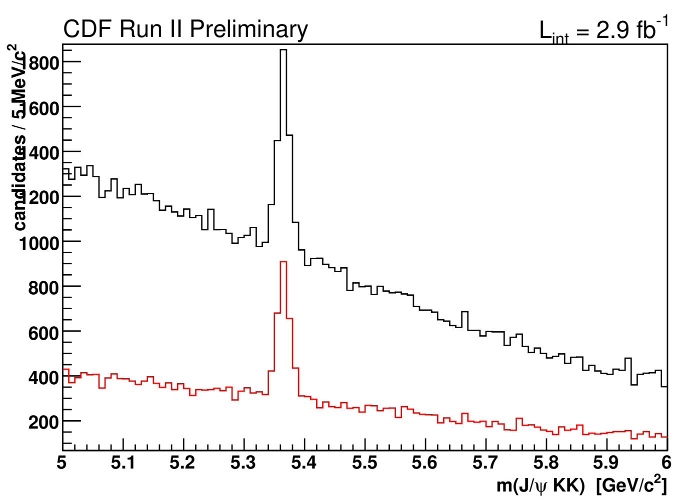


Figure 18: *Indication of a possible $B_s^0 \to J/\psi\phi$ signal with $J/\psi \to ee$ present in the Two Track Trigger sample. Black: no lepton required. Red: 1 CdfElectromagnetic Object associated to the $J/\psi$ tracks*

The selected events $B_s^0$ mass distribution with optimized cuts are shown in Figure 19 for both $B_s^0 \to \phi\phi$ and $B_s^0 \to J/\psi\phi$, with clear signal visible in both cases. For the former cuts reported in Table 3, leftmost column have been used, for the latter those reported in Table 4.

# 6 Measurement of the Signal Yields

Applying the optimized cuts the invariant mass distributions, $m_{KKKK}$ for the $B_s \to \phi\phi$ and $m_{\mu\mu KK}$ for $B_s \to J/\psi\phi$, are obtained (Figure 19). These provides us with a first insight on the background and signal composition.

In these distributions at least three components can be identified:

- **the signal** itself.
- **combinatoric background**: these are random combinations of charged tracks accidentally satisfying the selection requirements. They produce a continuous invariant $B_s$ mass distribution and we expect a smooth slowing decreasing distribution in the signal region. It is the more important source of background in our analysis.
- **physics background**: it is due to partially reconstructed heavy flavor decays or to an incorrect mass assignment to the tracks of other B meson decays (they are often referred to as reflections). We expect a distribution with a peak under the signal.

We evaluated the best parametrization of the components using the Monte Carlo simulation. Then, a fit on our data sample which takes into account all the identified components was performed to extract the signal yields. This procedure allowed us to fix some parameters in the function parametrizations and then to make a global fit with a limited number of free parameters.

## 6.1 $B_s \to J/\psi\phi$ events

We describe how the different components parametrizations were performed and we measure the events yield for the $B_s^0 \to J/\psi\phi$ events.

### 6.1.1 The signal

The signal has a width of around 10 MeV and it is parametrized with two gaussian having the same mean value but different resolutions (Figure 20). This choice is fairly standard and takes into account the detector effects that cause an additional spread in the tail distributions. The function used to parametrize the distribution is the

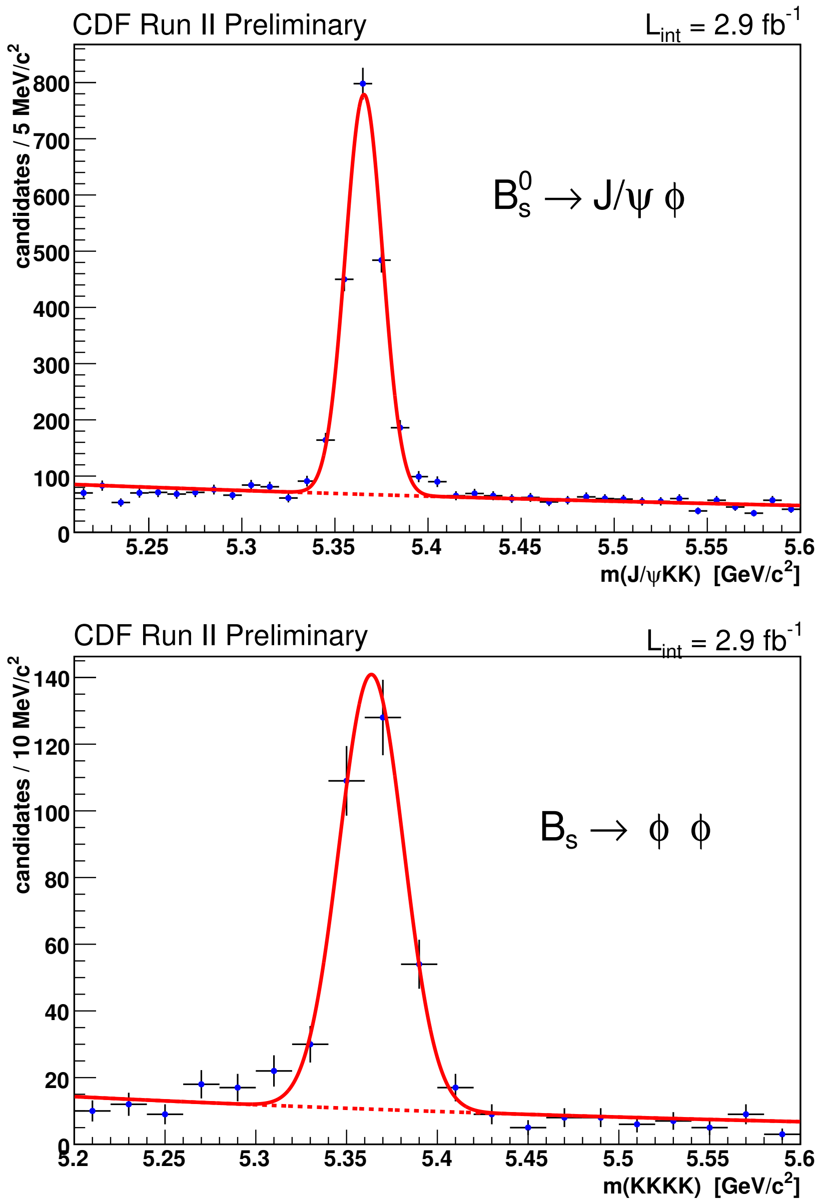


Figure 19: *Invariant mass distributions using the optimized selections.*

following:

$$G(x) = C_G \cdot f\frac{1}{\sqrt{2\pi}\sigma_1} \cdot e^{-\frac{(x-\mu)^2}{2\sigma_1^2}} + (1-f) \cdot \frac{1}{\sqrt{2\pi}\sigma_1 k} \cdot e^{-\frac{(x-\mu)^2)}{2\sigma_1^2 k^2}} \tag{1}$$

where $C_G$ is a multiplicative normalization constant, $f$ is the fraction of one gaussian component with respect to the other and $k$ is a multiplicative factor of the second Gaussian resolution. Fitting the Monte Carlo events of Figure 20 we obtained the parameters summarized in Table 5.

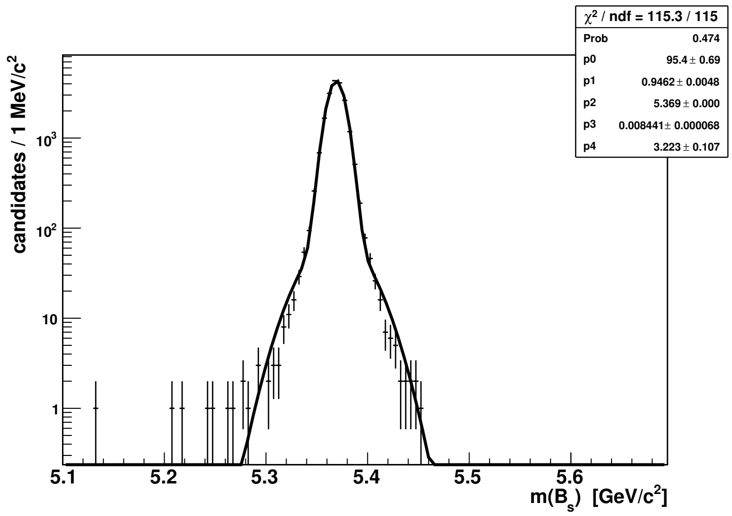


Figure 20: *Signal simulated using Monte Carlo. The y axis is in logarithmic scale.*

| parameter | value | error |
|---|---|---|
| $C_G$ | 95.40 | 0.70 |
| $f$ | 0.9462 | 0.00486 |
| $\mu$ | 5.36913 | 0.00007 |
| $\sigma_1$ | 0.00844 | 0.00007 |
| $k$ | 3.22 | 0.11 |

Table 5: *Fit parameter values for the signal simulated with MC.*

In the final fit of our data, the multiplicative factor $k$ and the fraction $f$ are fixed, while the other parameters are left free.

### 6.1.2 The combinatoric background

The combinatoric background is the more important contribution in this analysis within the considered mass window and its invariant mass distribution follows, with a good approximation, an exponentially decreasing behavior. In this case, we didn't perform a Monte Carlo study and a simple parametrization has been used instead.

### 6.1.3 The reflections

The more frequent decay that enters as a reflection in the invariant mass window of this decay is the $B_d \to J/\psi K^{*0}$ decay. It occurs when in the reconstruction of the $B_s \to J/\psi\phi$ decay, the daughter tracks of the $K^{*0} \to K\pi$ decay are assumed to be two kaons and an incorrect invariant mass is computed.
This component, simulated with Monte Carlo, can be parametrized with an asymmetric Gaussian and a decreasing exponential function expressed by:

for $x > \mu$:

$$R(x) = C \cdot \frac{2}{1 + [(f_G \cdot \frac{1}{\sqrt{2\pi}\sigma_2} + (1-f_G)\cdot\frac{b}{2}) \cdot \sqrt{2\pi}\sigma_1]} \cdot (f_G \cdot \frac{1}{\sqrt{2\pi}\sigma_2} \cdot e^{-\frac{(x-\mu)^2}{2\sigma_2^2}} + (1-f_G)\frac{b}{2} \cdot e^{-b(x-\mu)})$$

and for $x < \mu$:

$$R(x) = C \cdot [(f_G \cdot \frac{1}{\sqrt{2\pi}\sigma_2} + (1-f_G)\cdot\frac{b}{2}) \cdot \sqrt{2\pi}\sigma_1] \cdot \frac{2}{1 + [(f_G \cdot \frac{1}{\sqrt{2\pi}\sigma_2} + (1-f_G)\cdot\frac{b}{2}) \cdot \sqrt{2\pi}\sigma_1]} \cdot \frac{1}{\sqrt{2\pi}\sigma_1} e^{-\frac{(x-\mu)^2}{2\sigma_1^2}} \qquad (2)$$

where $C$ is the normalization constant, $f_G$ is the fraction of the Gaussian compared to the exponential, $\mu$ is the mean value and $\sigma_1$, $\sigma_2$ are the two resolutions of the Gaussian distributions, $b$ is the exponential parameter.

The reflection distribution and the fitted function are shown in Figure 21. The obtained fit parameter values are summarized in Table 6 and they show that this reflection has a distribution centered just below our signal.

| parameter | value | error |
|---|---|---|
| C | 8.41 | 0.20 |
| $f_G$ | 0.305 | 0.058 |
| $\mu$ | 5.363 | 0.0014 |
| $\sigma_1$ | 0.0209 | 0.0009 |
| $\sigma_2$ | 0.016 | 0.002 |
| b | 18.8 | 1.2 |

Table 6: *Fit parameter values for the reflection $B_d \to J/\psi K^{*0}$ simulated with Monte Carlo.*

The background fraction $f_{J/\psi K^{*0}} = N(B_d \to J/\psi K^{*0})/N(B_s \to J/\psi\phi)$ of $B_d \to J/\psi K^{*0}$ lying under the $B_s$ peak is estimated using:

$$f_{J/\psi K^{*0}} = \frac{f_d}{f_s} \frac{BR(B_d \to J/\psi K^{*0})}{BR(B_s \to J/\psi\phi)} \frac{BR(K^{*0} \to K\pi)}{BR(\phi \to K^+K^-)} \frac{\varepsilon_{TOT}^{J/\psi K^{*0}}(J/\psi\phi)}{\varepsilon_{TOT}^{J/\psi\phi}} \qquad (3)$$

where $\varepsilon_{TOT}^{J/\psi K^{*0}}(J/\psi\phi)$ is the trigger and selection efficiency of the $B_d \to J/\psi K^{*0}$ decays reconstructed as a $B_s \to J/\psi\phi$ one and $\varepsilon_{TOT}^{J/\psi\phi}$ is the trigger and selection efficiency for $B_s \to J/\psi\phi$, both estimated using Monte Carlo events. The other parameters are extracted from the PDG [11]; $f_d$ and $f_s$ are the production fractions of the $B_d$ and $B_s$ mesons.

From this formula we obtained $f_{J/\psi K^{*0}} = 0.0419 \pm 0.0093$; the large error is mostly due to the actual precision on the BR measurements and the $\frac{f_d}{f_s}$ uncertainty.

In the global fit of our data distribution, $f_{J/\psi K^{*0}}$ is fixed.

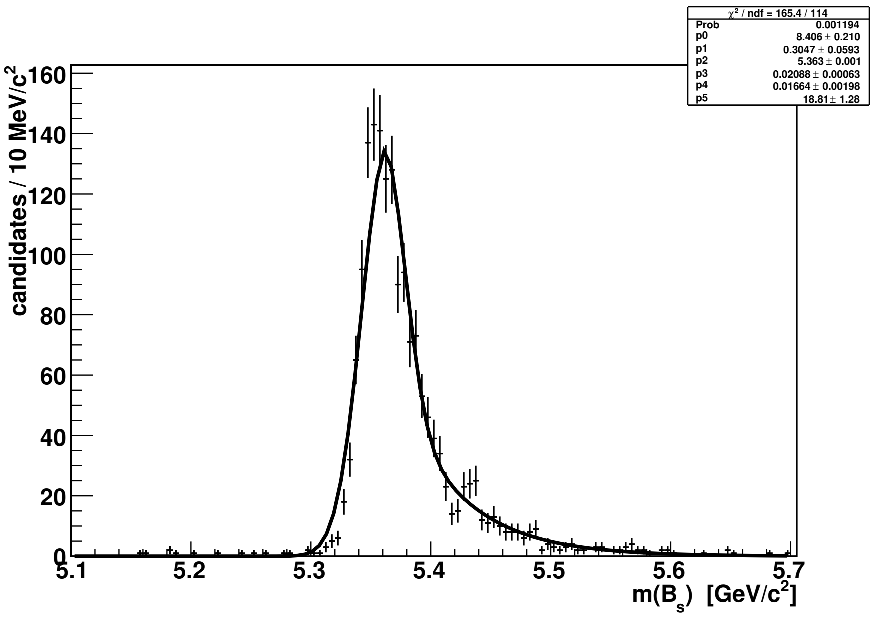


Figure 21: *The distribution of the reflection* $B_d \to J/\psi K^{*0}$.

### 6.1.4 Final fit

A global maximum likelihood fit is performed taking into account all the components described above. The function used to perform this fit is the following:

$$F(x) = C_{TOT} \cdot (frac \cdot (f\frac{1}{\sqrt{2\pi}\sigma_1} \cdot e^{-\frac{(x-\mu)^2}{2\sigma_1^2}} + (1-f) \cdot \frac{1}{\sqrt{2\pi}\sigma_1 k} \cdot e^{-\frac{(x-\mu)^2)}{2\sigma_1^2 * k^2}})+$$

$$(1-frac) \cdot (1-f_k)\frac{b}{e^{-bx_{MAX}} - e^{-bx_{MIN}}}e^{-bx} + (1-frac) \cdot f_k \cdot R(x)) \qquad (4)$$

where $k$ is fixed by MC; $R(x)$ is the function defined in equation 2, without the normalization factor $C$ and with the other parameters fixed by Monte Carlo simulations; $f_k = \frac{frac * f_{J/\psi K^*}}{1-frac}$ where $frac$ is the signal event fraction compared to the total number of events $n_{TOT}$ in the histogram of Fig.22. In this figure the fitted function of Eq.4 is shown together with the background components.

In conclusion, we obtain the number of $B_s \to J/\psi\phi$ events in our sample:

$$N_{J/\psi\phi} = frac \cdot n_{TOT} = 1766 \pm 48(\text{stat}) \qquad (5)$$

where the statistical uncertainty accounts for the uncertainty on both the signal fraction ($frac$) and the total number of events (the correlation is always negligeable). and for different trigger configurations we measure the fractions shown in Tab.7.

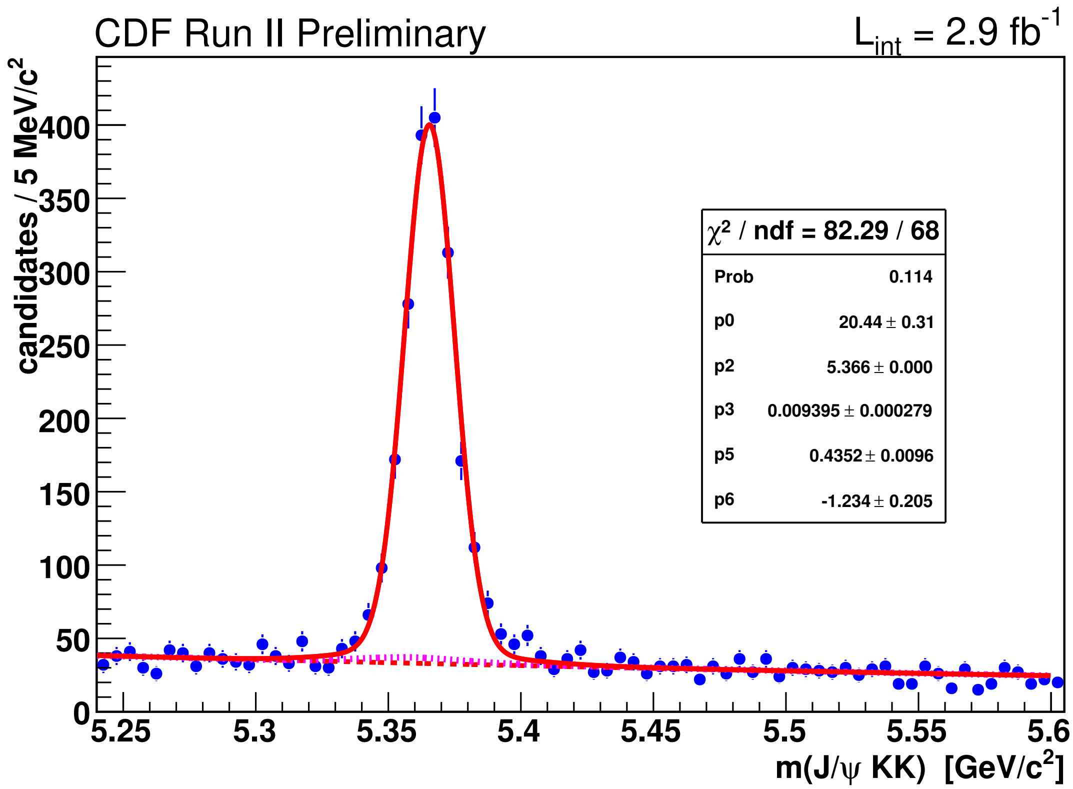


Figure 22: *Global fit of the $B_s \to J/\psi\phi$ invariant mass distribution. Red dashed: parametrization of the combinatoric background with a decreasing exponential. Pink dotted: the reflection of the $B_d \to J/\psi K^*$ decay. The signal is parametrized with two gaussian having the same mean value but different resolutions.*

| Trigger path | fractions |
|---|---|
| `HIGHPT` | $0.416 \pm 0.021$ |
| `ScA.not.HIGHPT` | $0.326 \pm 0.018$ |
| `LOWPT.not.ScA.not.HIGHPT` | $0.259 \pm 0.016$ |

Table 7: *Event fractions of different trigger configurations for $B_s \to J/\psi\phi$.*

## 6.2 $B_s \to \phi\phi$ events

### 6.2.1 The signal

The signal has a width of around 20 MeV and, as for the $B_s \to J/\psi\phi$, it is parametrized using two Gaussians with the same mean value but different resolutions (equation 1). The fit parameters obtained on the MC sample (Figure 23) are reported in Table 8.

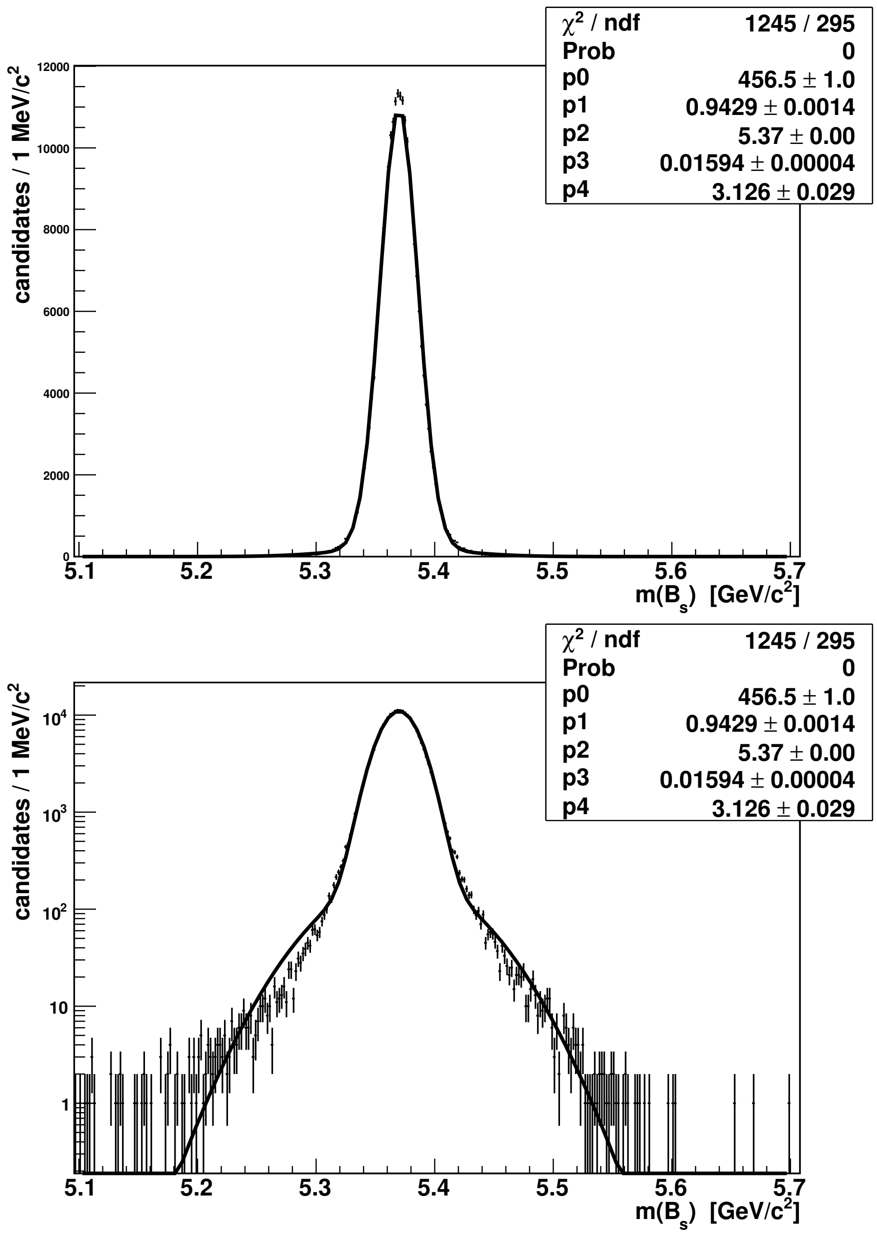


Figure 23: *$B_s$ invariant mass distribution simulated with MC, in linear (top) and logarithmic (bottom) scale.*

| parameter | value | error |
|---|---|---|
| $C_G$ | 456.5 | 1.0 |
| $f$ | 0.9429 | 0.0014 |
| $\mu$ | 5.36994 | 0.00004 |
| $\sigma_1$ | 0.015941 | 0.00004 |
| $k$ | 3.13 | 0.03 |

Table 8: *Fit parameters of the $B_s \to \phi\phi$ signal distribution simulated with MC.*

In the final fit on the data sample, the relative fraction of events of one gaussian with respect to the other and the multiplicative factor of the second Gaussian resolution are fixed.

#### 6.2.2 The combinatoric background

As in the $B_s \to J/\psi\phi$ decay, the combinatoric background is the more important background component in the invariant mass spectrum and it is parametrized with a decreasing exponential function.

#### 6.2.3 The reflections

The decays that could produce reflections in the $B_s$ mass window are:

$$B_d \to \phi K^* \to KKK\pi$$
$$B_s \to \bar{K}^* K^* \to \bar{K}\pi^- K\pi^+$$

These reflections occur when the $K^*$ is incorrectly reconstructed as a $\phi$.

The background contributions are calculated using:

$$N(B_d \to \phi K^*) = \frac{f_d}{f_s} \frac{BR(B_d \to \phi K^*)}{BR(B_s \to J/\psi\phi)} \frac{BR(K^* \to K\pi)}{BR(J/\psi \to \mu\mu)} \frac{\varepsilon_{TOT}^{\phi K^*}(\phi\phi)}{\varepsilon_{TOT}^{J/\psi\phi}} N(B_s \to J/\psi\phi) \quad (6)$$

$$N(B_s \to \overline{K^*}K^*) = \frac{BR(B_s \to \overline{K^*}K^*)}{BR(B_s \to J/\psi\phi)} \frac{BR(K^* \to K\pi)}{BR(J/\psi \to \mu\mu)} \frac{BR(K^* \to K\pi)}{BR(\phi \to KK)} \frac{\varepsilon_{TOT}^{\overline{K^*}K^*}(\phi\phi)}{\varepsilon_{TOT}^{J/\psi\phi}} \cdot N(B_s \to J/\psi\phi) \quad (7)$$

where $\varepsilon_{TOT}^{\phi K^*}(\phi\phi)$ and $\varepsilon_{TOT}^{\overline{K^*}K^*}(\phi\phi)$ are respectively the $B_d \to \phi K^*$ and $B_s \to \overline{K^*}K^*$ efficiency to be reconstructed as a $B_s \to \phi\phi$ decay. These efficiencies are evaluated using the Monte Carlo generated events. The number of $B_s \to J/\psi\phi$ events was calculated in the previous section and it is $N(B_s \to J/\psi\phi) = 1766 \pm 39$. Then, the number of reflection events is computed from Eq.6 and 7 and they are summarized in Table 9.

| reflection | $\varepsilon_{TOT}(\phi\phi)$ | number of events |
|---|---|---|
| $B_s \to \overline{K^*}K^*$ | $\sim 10^{-6}$ | 0 |
| $B_d \to \phi K^*$ | $0.000134 \pm 0.000002$ | $8 \pm 3$ |

Table 9: *Number of events and efficiencies for the $B_s \to \phi\phi$ reflections.*

Since the trigger and reconstruction efficiency of the $B_s \rightarrow \bar{K}^* K^*$ as a $B_s \rightarrow \phi\phi$, $\varepsilon_{TOT}(\phi\phi)$, is very low in the $B_s$ mass window, we neglected its contribution in our analysis.

The parametrization of the $B_d \rightarrow \phi K^*$ reflection has been studied with the Monte Carlo simulation. We implement a fit with an asymmetric gaussian and an exponentially decreasing function as in equation 2. The fit is shown in Fig.24 and its parameters

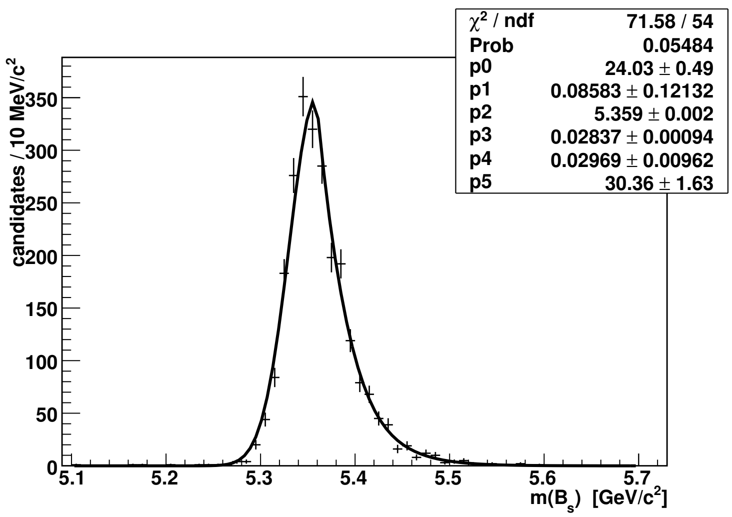


Figure 24: *Invariant mass distribution of $B_d \rightarrow \phi K^*$ events which pass the reconstruction selections of the $B_s \rightarrow \phi\phi$ decay.*

are summarized in Table 10.

| parameter | value | error |
|---|---|---|
| C | 24.03 | 0.49 |
| $f_G$ | 0.086 | 0.121 |
| $\mu$ | 5.359 | 0.002 |
| $\sigma_1$ | 0.0284 | 0.0009 |
| $\sigma_2$ | 0.030 | 0.010 |
| b | 30.4 | 1.6 |

Table 10: *Fit parameters values for $B_d \rightarrow \phi K^*$.*

### 6.2.4 Final fit

The global and final maximum likelihood fit on the data sample is performed taking into account all the signal and background components and using equation 4 with parameters and variables defined in analogous way to the $B_s^0 \rightarrow J/\psi\phi$ case. The number of signal events was extracted multiplying the fraction $frac$ for the total number of

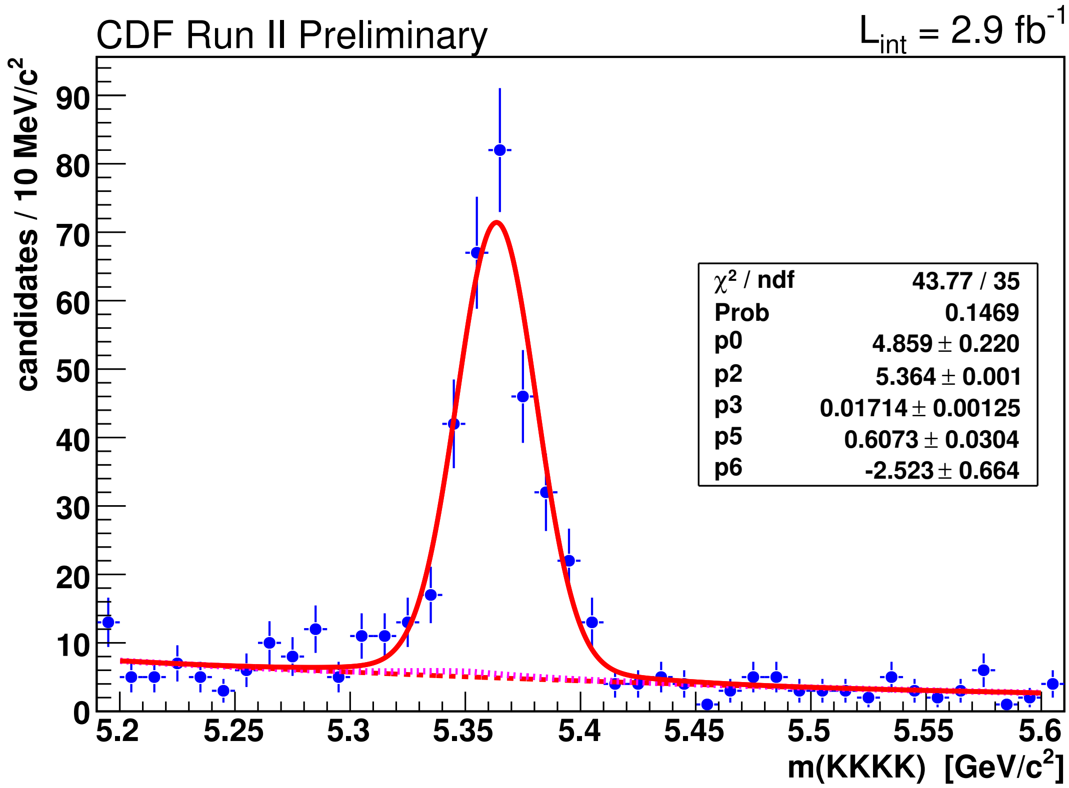


Figure 25: *Global fit of the $B_s \to \phi\phi$ invariant mass distribution. The red dashed line is the parametrization of the combinatoric background; the pink dotted line shows the small contribution (8 events) of the $B_s \to \phi K^*$ reflection. The signal is parametrized using two gaussian having the same mean value but different resolutions.*

events in the histogram in Figure 25.

The number of $B_s \to \phi\phi$ events is then determined as:

$$N_{\phi\phi} = 295 \pm 20(\text{stat}) \tag{8}$$

where the uncertainty takes into account the full correlation matrix of the fit results. In Table 11 we summarize the fractions of events for different trigger configurations.

# 7 Measurement of $BR(B_s^0 \to \phi\phi)$

The Branching Ratio (BR) of the decay $B_s \to \phi\phi$, normalized to the already measured BR($B_s \to J/\psi\phi$), can be evaluated using the following formula:

$$\frac{BR(B_s \to \phi\phi)}{BR(B_s \to J/\psi\ \phi)} = \frac{N_{\phi\phi}}{N_{J/\psi\phi}} \cdot \frac{\varepsilon_{TOT}^{J/\psi\phi}}{\varepsilon_{TOT}^{\phi\phi}} \cdot \frac{BR(J/\psi \to \mu\mu)}{BR(\phi \to KK)} \tag{9}$$

| Trigger path | fractions |
|---|---|
| HIGHPT | $0.394 \pm 0.048$ |
| ScA.not.HIGHPT | $0.377 \pm 0.048$ |
| LOWPT.not.ScA.not.HIGHPT | $0.223 \pm 0.037$ |

Table 11: *Fractions for the different trigger configurations for the $B_s \to \phi\phi$ decay.*

where $N_{J/\psi\phi}$ and $N_{\phi\phi}$ are respectively the number of $B_s \to J/\psi\phi$ events and the number of $B_s \to \phi\phi$ events in our sample; $\varepsilon^{J/\psi\phi}_{TOT}$ and $\varepsilon^{\phi\phi}_{TOT}$ are the combined trigger and selection efficiencies derived from MC simulation.

In the ratio of Eq.9 the uncertainties in the cross section of $B$ mesons hadronic production cancel out as well as several systematic effects due to the detector, allowing us to reduce the error on the measurement of the BR.
The $B_s \to J/\psi\phi$ decay is used in Eq.9 because it has a similar topology of the $B_s \to \phi\phi$ one; in particular it is characterized by the same number of decay vertexes and of charged tracks in the final state. The choice of the $B_s \to J/\psi\phi$ decay instead of the even more similar $B_d \to \phi K^*$ decay is motivated by the fact that in this way the uncertainties in the ratio of the production cross section of $B_s$ and $B_d$ do not enter in our formula. To obtain a sample with a good signal to background ratio, $J/\psi$ decays into two muons are selected with the request that at least one of the two muons is associated with a stub of the muon detectors. In this way the contribution of the $J/\psi \to ee$ decay is excluded from our sample. Furthermore the presence of muon stubs on both muons are not required to increases the statistics of the selected data.

# 8 Trigger and Selection Efficiencies

The ratio of the selection and the trigger efficiencies that enters in the BR measurement in principle could be estimated using events simulated by Monte Carlo. The efficiency is obtained computing the ratio between the number of events that satisfy the various trigger and selection criteria (with the same set of cuts used for the signal selection in the data) and the number of generated events. We actually use data sample as well to estimate some quantities not well modeled by MC.

As a first step, the trigger and selection efficiencies are estimated separately for different exclusive trigger configurations (see Tables 12 and 13).

The Monte Carlo is not able to simulate the various prescale factors of the different triggers and, as we have seen in Sec.3, the re-weighted Monte Carlo reproduces better the data. Therefore, we have to take into account the different prescales for the used trigger configurations while calculating the total efficiency of each $B_s$ decay.

| exclusive trigger configuration | $\varepsilon_i$ |
|---|---|
| HIGHPT | $0.003500 \pm 0.000042$ |
| ScA.not.HIGHPT | $0.002533 \pm 0.000036$ |
| LOWPT.not.ScA.not.HIGHPT | $0.004238 \pm 0.000046$ |
| global | $0.010271 \pm 0.000071$ |

Table 12: *Trigger and selection efficiencies of the $B_s \to J/\psi\phi$ for exclusive trigger configurations.*

| exclusive trigger configuration | $\varepsilon_i$ |
|---|---|
| HIGHPT | $0.003632 \pm 0.000013$ |
| ScA.not.HIGHPT | $0.002857 \pm 0.000012$ |
| LOWPT.not.ScA.not.HIGHPT | $0.004980 \pm 0.000016$ |
| global | $0.011468 \pm 0.000024$ |

Table 13: *Trigger and selection efficiencies of the $B_s \to \phi\phi$ for exclusive trigger configurations.*

Thus, the total efficiency is given by:

$$\varepsilon_{TOT} = \sum_i p_i \varepsilon_i \tag{10}$$

where $p_i$ and $\varepsilon_i$ are, respectively, the prescale factor and the efficiency of each exclusive trigger (in our case: `HIGHPT`, `ScA.not.HIGHPT` and `LOWPT.not.ScA.not.HIGHPT`). The fraction of data selected by a particular exclusive trigger is related to the prescale by

$$f_i = \frac{p_i \varepsilon_i}{\varepsilon_{TOT}} \tag{11}$$

The fractions of the different triggers were presented in Tables 7 and 11. The prescale factors $p_i$ depends only on the dataset and on the particular trigger configuration; so they are the same for the two decay modes under study. Therefore we estimated the ratio of prescales using the trigger fractions $f_i$ evaluated with the high statistics $B_s \to J/\psi\phi$ sample. This procedure allow us to obtain a smaller error on the total efficiencies ratio that would otherwise be dominated by the error on the fraction $f_i$ of $B_s \to \phi\phi$ events.

For what concerns the total efficiency of $B_s \to J/\psi\phi$, it is to be underlined that the Monte Carlo is not fully reliable for the simulation of the muon detectors. For this reason we evaluate the total efficiency for the $B_S \to J/\psi\phi$ as the product of a trigger and selection efficiency ($\varepsilon_{rec}^{J/\psi\phi}$), evaluated with the Monte Carlo, and a muon efficiency ($\varepsilon_\mu$) that is evaluated separately on the data, i.e.

$$\varepsilon_{TOT}^{J/\psi\phi} = \varepsilon_{rec}^{J/\psi\phi} \cdot \varepsilon_\mu$$

In the next section the procedure to estimate the muon efficiency will be explained. Using Eq.11 we calculate $\varepsilon_{rec}^{J/\psi\phi}$:

$$\varepsilon_{rec}^{J/\psi\phi} = p_{\texttt{HIGHPT}} \cdot \frac{\varepsilon_{\texttt{HIGHPT}}^{J/\psi\phi}}{f_{\texttt{HIGHPT}}^{J/\psi\phi}} \tag{12}$$

and the total efficiency for $B_s \to \phi\phi$ can be extracted from Eq.10 and it is

$$\varepsilon_{TOT}^{\phi\phi} = p_{\texttt{HIGHPT}} \cdot \sum_i \frac{p_i}{p_{\texttt{HIGHPT}}} \varepsilon_i \tag{13}$$

where $\frac{p_i}{p_{\texttt{HIGHPT}}}$ are estimated from the $J/\psi\phi$ data sample using the following equation:

$$\frac{p_i}{p_{\texttt{HIGHPT}}} = \frac{\varepsilon_{\texttt{HIGHPT}}^{J/\psi\phi} \cdot f_i^{J/\psi\phi}}{\varepsilon_i^{J/\psi\phi} \cdot f_{\texttt{HIGHPT}}^{J/\psi\phi}}$$

The final expression for the efficiency ratio is:

$$\frac{\varepsilon_{rec}^{J/\psi\phi}}{\varepsilon_{TOT}^{\phi\phi}} = \frac{\frac{\varepsilon_{\texttt{HIGHPT}}^{J/\psi\phi}}{f_{\texttt{HIGHPT}}^{J/\psi\phi}}}{\varepsilon_{\texttt{HIGHPT}}^{\phi\phi} + \frac{\varepsilon_{\texttt{HIGHPT}}^{J/\psi\phi} \cdot f_{\texttt{LOWPT}}^{J/\psi\phi}}{\varepsilon_{\texttt{LOWPT}}^{J/\psi\phi} \cdot f_{\texttt{HIGHPT}}^{J/\psi\phi}} \cdot \varepsilon_{\texttt{LOWPT}}^{\phi\phi} + \frac{\varepsilon_{\texttt{HIGHPT}}^{J/\psi\phi} \cdot f_{\texttt{ScA}}^{J/\psi\phi}}{\varepsilon_{\texttt{ScA}}^{J/\psi\phi} \cdot f_{\texttt{HIGHPT}}^{J/\psi\phi}} \cdot \varepsilon_{\texttt{ScA}}^{\phi\phi}} = 0.906 \pm 0.030$$

From this result we see that the $B_s \to \phi\phi$ combined trigger and recontruction efficiency appears to be greater than the $B_s \to J/\psi\phi$. This can be likely be explained by the particular kinematics of the $B_s \to \phi\phi$ decay with both mesons in turn decaying with a very low Q value and because the efficiency correlations between the four tracks in general tend to favor $B_s \to \phi\phi$ decay over $B_s \to J/\psi\phi$. We finally note that the uncertainty associated with the efficiency ratio is statistical in nature being completely dominated by the statistical uncertainty of the extraction from data itself of the "prescales factors" $p_i$.

# 9 Muon Efficiency

As explained in the previous section, the efficiency of the signal selection for $B_s \to J/\psi\phi$ is separated into a trigger and selection efficiency (evaluated with the Monte Carlo) and the efficiency of the request of the muon presence, which is estimated on the data.

The requirement on the muons for the channel $B_s^0 \to J/\psi\phi$ is that the $J/\psi$ candidates have at least one of the two tracks with a match in the muon detectors. This is implemented using the *HasMuon* flag of the *BStntuples*. Therefore, it is necessary to estimate the efficiency of this request, $\varepsilon_\mu^{TOT}$, which has been computed as a function of the muon transverse momentum, in two pseudo-rapidity regions corresponding to the CMU and CMX detectors. In a second step, this function is used to calculate the mean efficiency for selecting at least one muon using the $p_T$ muon spectrum provided by the Monte Carlo simulation of the $B_s^0 \to J/\psi\phi$ decay.

## 9.1 Efficiency of requiring the $HasMuon$ flag

We choose to evaluate the efficiency on an inclusive sample of $J/\psi \to \mu\mu$ collected through the Two Tracks Trigger. In the previous analysis [1] we used the abundant prompt $J/\psi$ peak in the sideband of our $B_s^0 \to J/\psi\phi$ signal. This is not any more possible since in the current *BStnuple*, due to the mass constraint used in the reconstruction, there is no usable sideband for background subtraction, thus we used the inclusive $J/\psi$ sample skimmed from the complete TTT dataset. Using data from the TTT guarantees us to be under the same exact trigger prescale conditions and to be free of muon trigger related bias (these conditions would not be satisfied using the $DI\_MUON$ trigger).

After imposing the following simple cuts a clean $J/\psi$ peak is visible as shown in Fig. 26:

- $L_{xy} > 200\mu m$ for the two track vertex;
- $\chi^2 < 5.0$ for the two track vertex;
- $p_T > 1.5$GeV/$c$ for both tracks;
- 1 track associated with a muon stub (*HasMuon* flag).

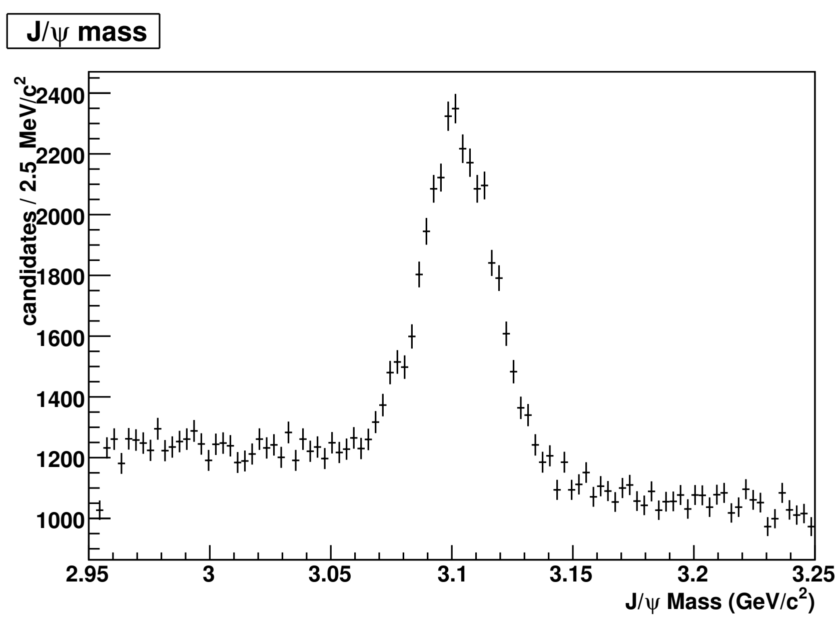


Figure 26: *$J/\psi$ invariant mass distribution after the preliminary cuts.*

The efficiency of the requirement of at least one muon, $\varepsilon_\mu$, was derived as a function of the muon $p_T$ and in two ranges of pseudorapidity $\eta$. We obtained two histograms showing the efficiency $\varepsilon_\mu$ as a function of the muon $p_T$, one for CMU ( $0.0 <\mid \eta \mid< 0.6$) and the other for CMX ( $0.6 <\mid \eta$). The muon efficiency as a function of $p_T$

was calculated dividing, bin by bin, two sideband subtracted histograms of the $p_T$ distribution for events that satisfy the request to have two muons or at least one muon and using the following formula [12]:

$$\varepsilon_\mu = \frac{N_{2\mu}}{N_{2\mu} + N_{1\mu}} \tag{14}$$

where $N_{1\mu}$ and $N_{2\mu}$ are, respectively, the number of events that has exactly one muon and the number of events with two identified muons. Since $N_{1\mu}$ and $N_{2\mu}$ are statistically independent, the formula used to evaluate the error in each single $p_T$ bin is:

$$\sigma_\varepsilon = \frac{[\sigma^2_{N_{2\mu}}(1-\varepsilon)^2 + \sigma^2_{N_{1\mu}} \cdot \varepsilon^2]^{1/2}}{N_{2\mu} + N_{1\mu}} \tag{15}$$

where $\sigma_{N_{2\mu}}$ and $\sigma_{N_{1\mu}}$ are the errors evaluated from the sum in quadrature of the poisson errors of the sideband and peak histograms.

The $J/\psi$ signal peak with two identified muons is shown in Fig. 27 along with the actual sideband mass regions: $M_{\mu,\mu} \in [2.985, 3.015] \cup [3.185, 3.215]\text{GeV}/c^2$. The signal peak region (60 MeV/$c^2$ wide) is defined as $M_{\mu,\mu} \in [3.072, 3.132]\text{GeV}/c^2$, corresponding approximately to a $\pm 2\sigma$ region.

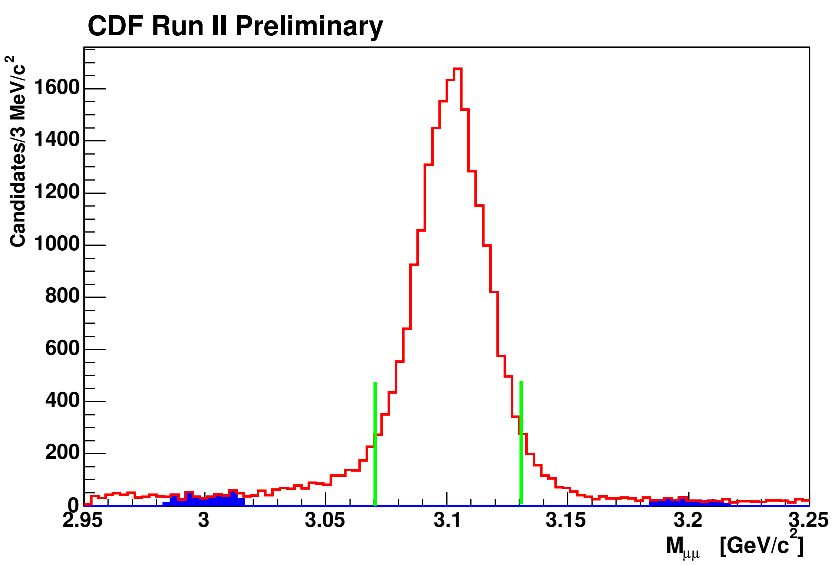


Figure 27: *$J/\psi$ invariant mass distribution with 2 identified region. Side-bands are highlighted in blue.*

We parametrize the efficiency as a function of $p_T$ obtained for both the CMU and CMX regions (see Figure 28) with a sigmoid function whose parameters are determined by a $\chi^2$ fit using Minuit:

$$\varepsilon(p_T) = \frac{A}{1 + e^{[B(p_T + C)]}} \tag{16}$$

The efficiency histograms with overlaid fitted function are reported in Fig. 28 for CMU and CMX regions and for the complete inclusive $J/\psi$ sample without a pseudo-rapidity binning in Fig. 29. The simple functions reproduce the observed efficiency curves with good $\chi^2$ (probabilities of 30%, 50% and 80% respectively for CMU, CMX and combined). As expected, due to the additional material before the CMX detectors, and to their overall reduced acceptance, the efficiency turn-on happen at higher transverse momentum and shows a lower plateau value. The fitted parameters are reported in Table 14.

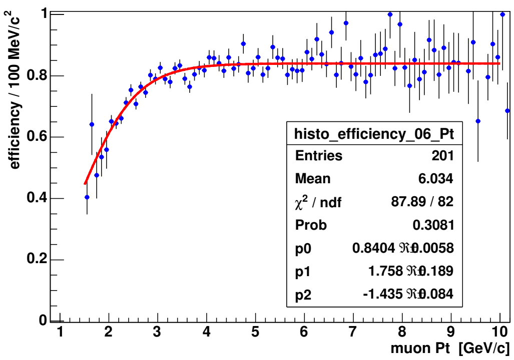

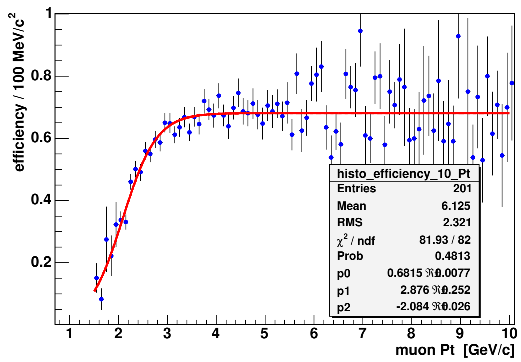


Figure 28: *Efficiencies as a function of muon transverse momentum: distribution for CMU (left) and CMX (right) muons. All these distributions are fitted with a sigmoid function.*

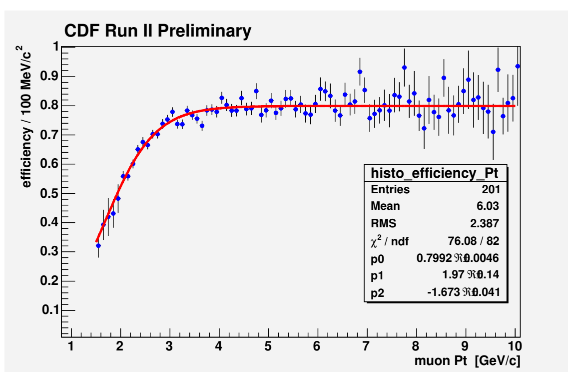


Figure 29: *Efficiencies as a function of muon transverse momentum: average efficiency for both CMU and CMX detectors in the inclusive TTT $J/\psi$ sample. The fitted sigmoid function is overlaid.*

We have checked the stability of the $p_T$ parametrization of the muon efficiency using a different good run list where CMU and CMX bits were requested. We did not find any significant change in the fitted parameters. This is expected since the additional integrated luminosity is less than 5%. Additionally the muon system is often declared

| | A | B | C |
|---|---|---|---|
| CMU | 0.8404± 0.0057 | 1.76 ± 0.19 | -1.435 ± 0.084 |
| CMX | 0.6815± 0.0077 | 2.88 ± 0.25 | -2.084 ± 0.026 |
| average | 0.7992± 0.0046 | 1.97 ± 0.14 | -1.673± 0.041 |

Table 14: *Parameter values of the sigmoid functions used to fit the muon efficiency distributions of Fig.28 and 29.*

bad at very high luminosity and often a significant part of the detector keep working. We have also tried to use a different sideband (i.d. shifted by 15 MeV/$c^2$ corresponding to $1\sigma$ of the $J/\psi$ mass resolution) and found results consistent with those of Table 14 within a fraction (1/3) of their statistical uncertainty.

## 9.2 Muon Efficiency vs $\phi$ and $\eta$

Following exactly the same path as above we studied also the muon identification efficiency as a function of other kinematical parameters of the muons, namely as a function of $\phi$ and $\eta$. We present in Fig. 30 the relevant results.

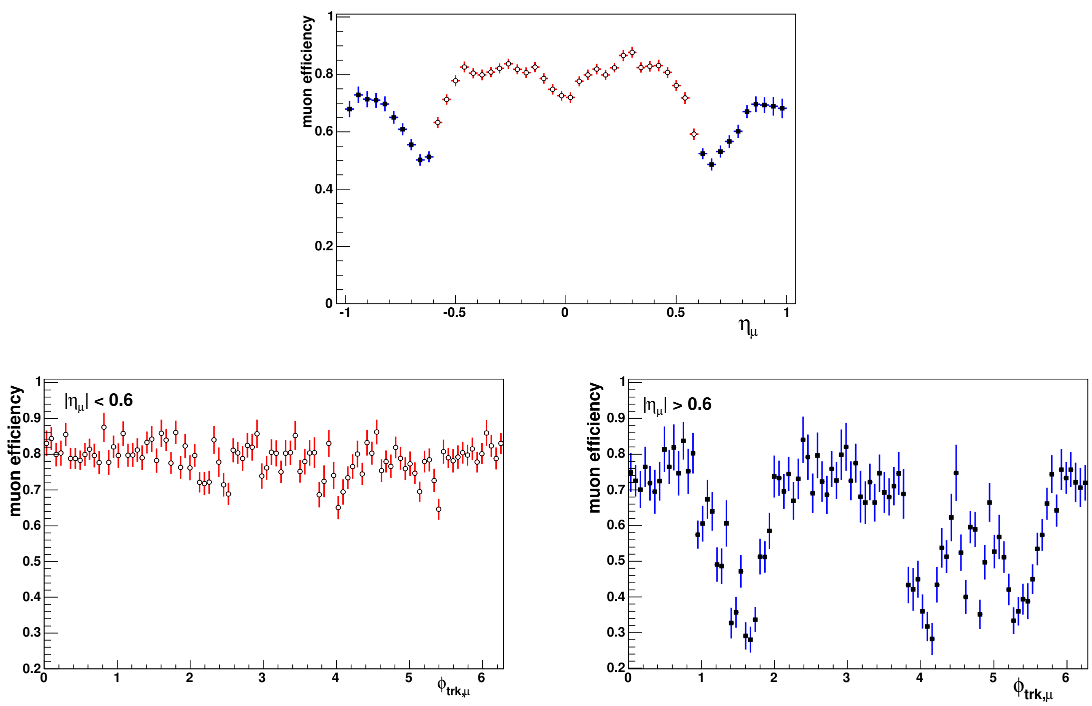


Figure 30: *Efficiencies as a function of $\eta$ (upper) and $\phi$ for CMU (left-bottom) and CMX (right-bottom) muons.*

We notice that in both views significant structures are visible, in particular in the transition between CMU and CMX, and, in the $r-\phi$ view, in the miniskirt region of the CMX detector. Clearly an optimal strategy should consider a parametrization in both views and with a sufficiency number of bins to capture all of the structures. Since, on the other hand, he expect the same azimuthal angle distribution for inclusive $J/\psi$ sample and the signal sample we can ignore the $\phi$ efficiency dependence. We demonstrate this by comparing the unbiased muon track $\phi$ distribution in the $J/\psi$ sample, obtained requiring that the other leg was positively identified, with the muon track $\phi$ distribution in the $B_s^0 \to J/\psi\phi$ Monte Carlo simulation without requirements on muon identification. We observe in Fig. 31 that the $J/\psi$ sample muons, being selected by the same trigger as our primary data shows exactly the same biases (likely due to the silicon requirements in the trigger). Likewise we also show the $\eta$ distribution and notice again a fair agreement between the two distributions. The latter observation convince us that a parameterization in just two $\eta$ regions will be accurate enough to calculate the average muon efficiency.

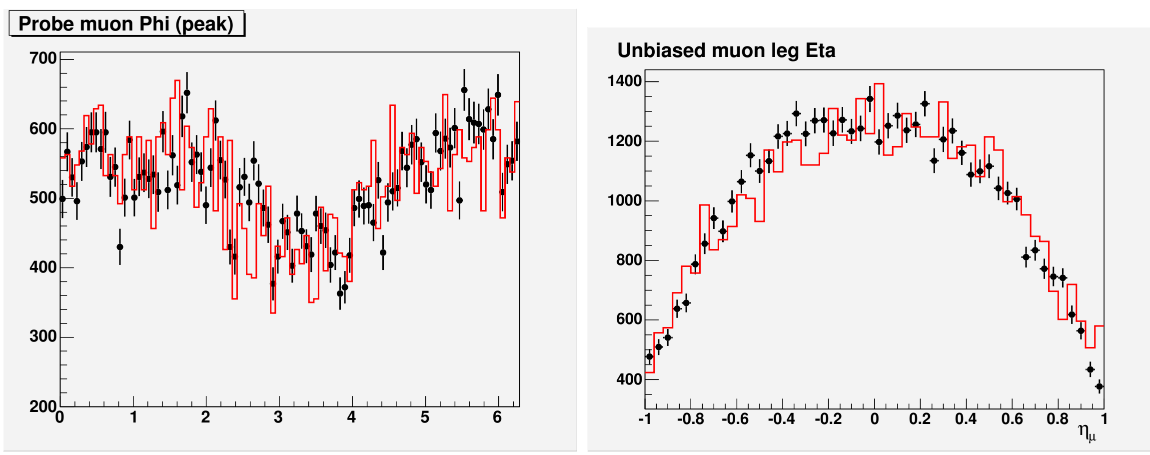


Figure 31: *Left: Muon track $\phi$ distribution for inclusive $J/\psi$ sample (points) and $B_s^0 \to J/\psi\phi$ MC (red histogram); Right: Muon track $\eta$ distribution for inclusive $J/\psi$ sample (points) and $B_s^0 \to J/\psi\phi$ MC (red histogram).*

Another interesting comparison can be performed between the $J/\psi$ $p_T$ and $\Delta\phi$ between the two muons, Fig. 32. We see that the inclusive $J/\psi$ sample represent a reasonable match to the expected characteristic of the $B_s^0 \to J/\psi\phi$ one. Moreover we notice that due, to the rather low momentum, of the $J/\psi$ the $\Delta\phi$ between the two muon legs is rather wide. This further justify the assumption we will make in the following that the muon identification efficiencies for the first and the second muon are to a good degree independent of each other.

## 9.3 Total Muon Efficiency

Using the muon efficiency as a function of $p_T$ and the $p_T$ spectrum of muons from simulated $B_s \to J/\psi\phi$ decays after trigger and kinematics selection, but no muon identification requirement, we calculate the average efficiency in our sample for finding

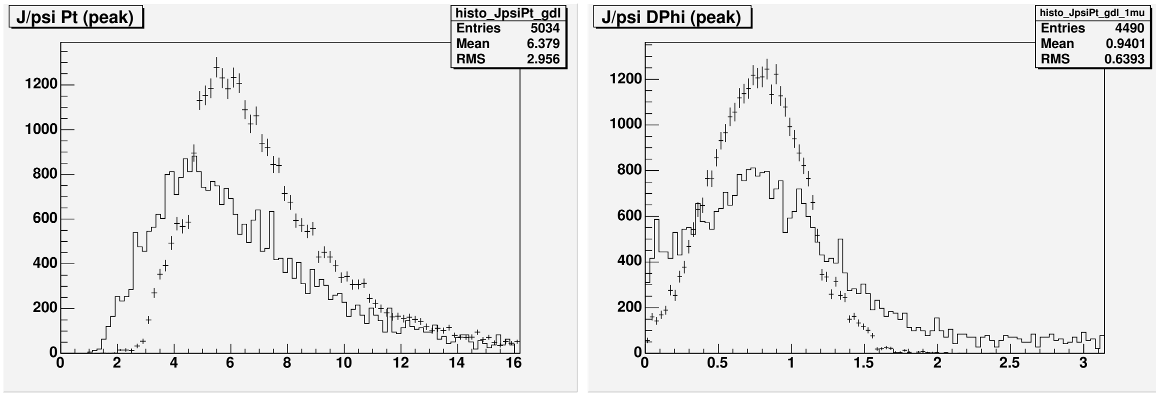


Figure 32: *$J/\psi$ $p_T$ and $\Delta\phi$ between the two muons for inclusive $J/\psi$ sample (points) and $B_s^0 \rightarrow J/\psi\phi$ MC (histogram)*

at least one of the $J/\psi$ muon legs with a matching stub in the muon detectors (HasMuon flag in the BsNtuple). Additionally, since the muon statistics is very low below 1.5 GeV/$c$ and the details of the efficiency turn-on at very low transverse momentum might be a source of systematic uncertainty, we introduce the further selection requirement of asking for muon stubs only for $J/\psi$ tracks with $p_T > 1.5$GeV/$c$. This additional requirement with respect to those in Table 4 affects in a negligeable ($< 0.1\%$)way the $B_s^0 \rightarrow J/\psi\phi$ candidate selection in data.

Assuming the efficiency for the first and second muon to be uncorrelated we obtain the per event efficiency for reconstructing at least 1 muon among the two $J/\psi$ decay tracks using the following formula:

$$\varepsilon_{\mu,\ i}^{TOT} = \varepsilon(p_{T1})_i \cdot [1 - \varepsilon(p_{T2})_i] + \varepsilon(p_{T2})_i \cdot [1 - \varepsilon(p_{T1})_i] + \varepsilon(p_{T1})_i \cdot \varepsilon(p_{T2})_i \tag{17}$$

where $(p_{T1,2})_i$ are the transverse momenta of the two muon tracks (1,2) from the i-th $J/\psi$ candidate decay, and the efficiencies are the CMU or CMX ones according to the muon pseudo-rapidity. The average of the per event efficiency over all the $J/\psi$ candidates in the $B_s \rightarrow J/\psi\phi$ Monte Carlo sample, will give the searched for efficiency. The MC distribution of this efficiency is shown in Fig. 33, using the two $p_T$-dependent turn-on curve in Fig. 28.

Including also the statistical uncertainty obtained by taking into account turn-on parameter fit uncertainties and their correlation we thus obtain: begindisplaymath

$$\varepsilon_{\mu}^{TOT} = 0.8695 \pm 0.0044(\text{stat}).$$

If the average efficiency were used the result would be:

$$\varepsilon_{\mu}^{TOT} = 0.8771 \pm 0.0035(\text{stat}).$$

corresponding to a relative change of just 0.9%.

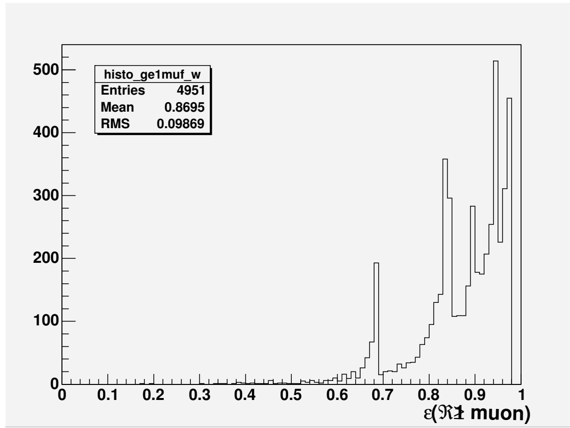


Figure 33: *Per event efficiency calculated on $B_s^0 \to J/\psi\phi$ MC using data parameterization*

## 9.4 Systematic Uncertainty on Muon Efficiency

To investigate the effects of both un-accounted for sources of correlation and background subtraction we performed the same analysis and calculation using the muon identification efficiency obtained from the muons in the $B_s^0 \to J/\psi\phi$ simulation. We derived muon identification efficiency as a function of muon transverse momentum using the MC truth information and checking the *HasMuon* flag. We find that the same functional form used for data is adequate to describe also the Monte Carlo efficiency. As expected the efficiency curve parameters are different in the MC, in particular the plateau values. We notice however that both the shape as a function of $p_T$ and as a function of $\eta$ as well as of $\phi$ are fairly similar to what we observe in data, giving further confidence on our data-driven determination, see Fig. 35.

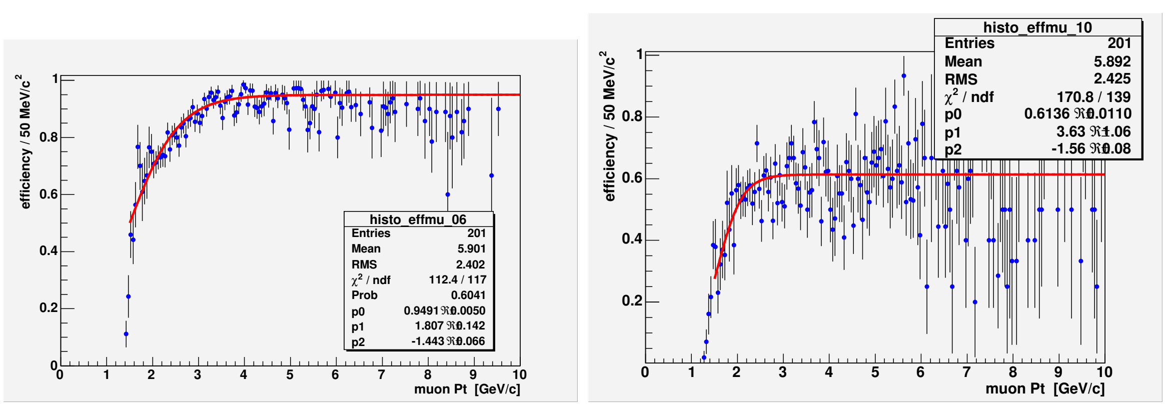


Figure 34: *Efficiencies as a function of muon transverse momentum: distribution for CMU (left) and CMX (right) muons from the Monte Carlo Simulation with overlaid fit.*

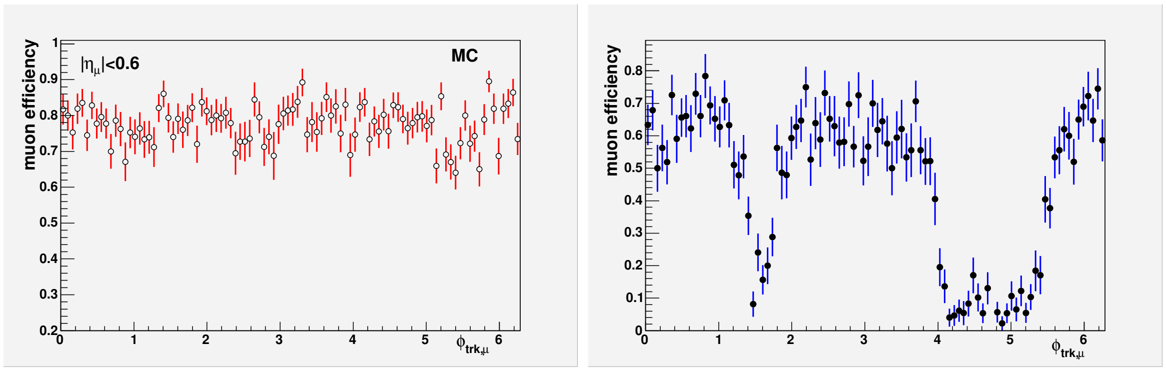


Figure 35: *Efficiencies as a function of $\phi$ for CMU (left) and CMX (right) muons.*

We can therefore derive the true efficiency (in our MC) for identifying 1 or more muons after all selection cuts $\varepsilon_\mu^{MC} = N_M^{\geq 1mu} C/N_{MC}$, where $N_M^{\geq 1mu} C$ is just the number of MC events surviving cuts with at least 1 muon identified and $N_{MC}$ is the number of MC events surviving cuts. This is

$$\varepsilon_\mu^{MC} = 4490/4951 = 0.9069 \pm 0.0041(\text{stat}) \tag{18}$$

to be compared with the equivalent number derived from the $p_T$-$\eta$ parameterization:

$$\varepsilon_\mu^{TOT,MC} = 0.9145 \pm 0.0046(\text{stat}) \tag{19}$$

that shows a shift from the true value which is barely significant and represents a 0.8% relative change. Had we used for the calculation the average efficiency in MC we would have obtained a relative shift of 1.1%.

By comparing the result above with the difference in muon average efficiency between the $\eta$-dependent and $\eta$-independent case described in the preceding section we conclude that missing correlations might at most have an effect equivalent to that. Since other sources of systematics (like the effect of bad detector status, or sideband definition) have proved to be negligeable we assign as a systematics uncertainty to the muon efficiency the full difference in central values obtained when using the average efficiency or the $\eta$-dependent one. The final result we will use for the BR determination is thus:

$$\varepsilon_\mu^{TOT} = 0.8695 \pm 0.0044(\text{stat}) \pm 0.0075(\text{syst}). \tag{20}$$

# 10 Systematic Uncertainties

This section lists and describes the main systematic effects that we take into account to determine the systematic uncertainty on the Branching Ratio.
They are:

- uncertainties on the number of events obtained in Sec.6 and due to:

  - the variation in the fit mass range;
  - the parametrization of the signal with one or two gaussian functions.

- uncertainties on the background subtraction;
- uncertainty on the muon efficiency;
- uncertainty on the ratio of the trigger and selection efficiencies due to effects not considered in the Monte Carlo simulation, such as:
  - the polarization of $B_s \to J/\psi\phi$ and $B_s \to \phi\phi$ and the related average lifetime differences between the two decay channels;
  - the $p_T$ spectra;
  - the effect due to the different particles types involved in the final states ($\mu\mu KK$ and $KKKK$) related to the particles dependence of the XFT efficiency.
- uncertainty due to the Branching Ratio of the normalization channel.

The strategy used to estimate these errors is presented below. The contribution of any single error to the total uncertainty on the BR determination is summarized at the end of the section.

## 10.1 Systematic uncertainty on the number of events

### 10.1.1 Fit range

We study the effect of the different range of $B_s$ invariant mass used for the fit. The range used to fit over the signal is, respectively, [5.20, 5.60] GeV/$c^2$ for the $B_s \to \phi\phi$ and [5.23, 5.60] GeV/$c^2$ for the $B_s \to J/\psi\phi$. The upper limit is chosen considering the presence of possible reflections of the $\Lambda_b$ that we do not know well enough, while the lower limit at 5.2 GeV/$c^2$ is due to the possible presence of other partially reconstructed decays for lower values of invariant mass. We used different lower limits for the fit range of the two decays because the fit of the $B_s \to J/\psi\phi$ decay has a $J/\psi$ mass constraint and thus a narrower mass resolution. In this latter case the default lower mass range is set at the $B_s^0$ mass minus 1 pion mass.

We have investigated the changes in the signal yields by varying the lower mass range. We find a significant effect in particular in the $B_s^0 \to \phi\phi$ case. While there is no significant structure emerging from the background there are several bins of the histograms that might suggest the presence of some satellite peak. There is no known background that might really produce peaks there as has been studied from simulation. As an example $B_s^0 \to K^{*0}\bar{K}^{*0}$, $B^0 \to \rho^0\rho^0$, $B^0 \to \rho^0 K^{*0}$ modes all produces bumps in the high mass side of the peak since we reconstruct the decay in the hypothesis of 4 Kaons in the final states while these modes only have no or few Kaons. Furthermore the selection efficiency for there modes are very low due to the two $\phi$ mass window we exploit in the $B_s^0 \to \phi\phi$ reconstruction. However for the sake of determining the systematics induced by the possible presence of an unknown peaking background on the low mass side of the signal we have introduced a second signal peak in our fit parametrization and evaluated the difference induced in the signal yield. In this way we obtain a fit with a somewhat improved $\chi^2$ probability and a signal yield differing from the default one by 8 events, consistent with what we find by varying the lower fit range from 5.2 GeV/$c^2$ to 5.23 GeV/$c^2$(9 events). We conclude that a systematic due to possible unknown sources of backgrounds might be conservatively assigned by taking the biggest of the two changes. The systematic uncertainty will be then : $\Delta N_{\phi\phi} = 9$.

#### 10.1.2 Signal parametrization

The second effect concerns the assumed shape for the signal which was derived from MC simulation. We assign a systematic error that arise from the use of a signal parametrization with a single Gaussian instead of two with the same mean value and a different resolution. In this case the bias is calculated from the difference in the number of events as obtained by the two parametrizations and we obtain: $\Delta N_{\phi\phi} = 8$ e $\Delta N_{J/\psi\phi} = 41$.

#### 10.1.3 Total uncertainties

The overall uncertainties that take into account these two effects and enter into the determination of the Branching Ratio are derived by adding in quadrature the above uncertainties: $\Delta N_{\phi\phi}(syst) = 12$ e $\Delta N_{J/\psi\phi}(syst) = 41$. These correspond to a relative uncertainty on Branching Ratios of respectively 4.1% and 2.3%.

### 10.2 Uncertainties on the background subtraction

We study the effect due to the error in quantifying the number of events of the reflections in the fit. The dominant contributions on this error come from the error on the Branching Ratio of $B_s \to J/\psi\phi$ and on the ratio of $\frac{f_s}{f_d}$, leading to a variation of 38% in the background subtraction.
The obtained systematic errors are therefore: $\Delta N_{\phi\phi} = 2$ e $\Delta N_{J/\psi\phi} = 13$.

### 10.3 $\eta$ dependence of $\varepsilon_\mu$

The effect of using an $\varepsilon_\mu$ parametrization as a function of the pseudorapidity as well has been estimated. The differences between the obtained result and that using the average parametrization is used as a systematic uncertainty on the muon efficiency. From eq. 20 we derive a relative uncertainty on the Branching Ratio of 0.5%:

## 10.4 Uncertainty on the trigger and selection efficiencies ratios

### 10.4.1 Polarization and lifetime values in Monte Carlo

Possible effects not included in the Monte Carlo simulation should be studied as possible contributions to the systematic error. We examined is the effect due to the polarizations of the $B_s \to \phi\phi$ and $B_s \to J/\psi\phi$ decays. In the used Monte Carlo, the decay amplitudes were set in such a way that all the final state polarizations have the same probability. To study the systematic effect of this assumption, we used in the Monte Carlo for the $B_s \to J/\psi\phi$ decay the measured polarization from CDF, while for the $B_s \to \phi\phi$ decay we used the polarization values of the very similar decay $B_d \to \phi K^*$ [5].

We assume as a systematic uncertainty the difference between the efficiency ratios with and without the polarization. We observe a similar effect for both $B_s^0 \to J/\psi\phi$ and $B_s^0 \to \phi\phi$ decays, a relative difference in the efficiency of respectively 7% and 6%. Since no experimental information on $B_s^0 \to \phi\phi$ polarization is available assigned the full effect as a systematic seems a reasonable choice. On the other end for $B_s^0 \to J/\psi\phi$ one could probably reduce this uncertainty in the future by making a less extreme variation. One should mention also that we are not currently assigning any systematic for lifetime since this should cancel to first order in the ratio. However the average effective lifetime in each mode depends on the true value of the $B_s^0$ lifetime difference ($\Delta\Gamma_s$), the value of the transverse perpendicular amplitude and the size of the $B_s^0$ mixing phase. Assuming vanishing $B_s^0$ mixing phase the average lifetime change by less than 4% between the fully longitudinally polarized case (as expected in naive models of polarization) and the "realistic" $B^0 \to \phi K^{*0}$ case. So we conclude that the 7% systematic uncertainty on the $B_s^0 \to J/\psi\phi$ polarization is sufficienctly conservative to cover also polarization induced lifetime difference between the $B_s^0 \to J/\psi\phi$ and $B_s^0 \to \phi\phi$ modes.

### 10.4.2 Particle dependent XFT efficiency

A possible large source of systematic in the relative acceptance corrections, can arise from differences in the XFT efficiency for charged kaons and muons, due to the different specific ionization of the two particles in the COT volume. Charged muons in the typical momentum range of the $\phi$ and $J/\psi$ decay products, tend to ionize more than charged kaons. The consequence is a larger pulse width for muons compared to kaons and then a larger number of hits in the COT chamber. Due to the requirements on the number of Axial COT hits per segement imposed by the XFT trigger, this can in turn reflect in a different efficiency for kaons and muons. This effect, is not reproduced in the simulation, and will not cancels in the efficiency ratios given above, resulting in a bias in the measurement of the relative branching fractions.

The scale factor for XFT efficiency in data and MC for kaons and pions as been studied extensively in [13] and never repeated again, to our knowledge. We use the numbers contained in [13] for the latest of the data-taking periods considered there, and apply those to out much larger dataset. Since we use old numbers we conservatively assign a systematics equivalent to half of the estimated shift.

To make this estimate we identify the two tracks that fired the trigger, among the four in our candidates, reproducing the trigger algorithm appropriated to our triggers. We then assign a weight to the event based on whether the track is a muon or is a kaon. Based on [13] numbers we expect then that the $B_s^0 \to J/\psi\phi$ efficiency has to be reduced by 9.96% and the $B_s^0 \to \phi\phi$ efficiency by 16.7%. Notice that among the $B_s^0 \to J/\psi\phi$ simulated events we find that 58% have 1 muon and 1 Kaon triggering while in 37% of the cases two muons trigger. We will then apply a correction to the efficiency ratio from Monte Carlo of 8.1% and assign a relative uncertainty of 4.0 % to the Branching Ratio measurement due to particle dependent trigger efficiency effects.

| | $B_s^0 \to \phi\phi$ | $B_s^0 \to J/\psi\phi$ |
|---|---|---|
| | $\Delta N_{\phi\phi}/N_{\phi\phi}$ | $\Delta N_{J/\psi\phi}/N_{J/\psi\phi}$ |
| fit range | 3% | - |
| signal parametrization | 3% | 2% |
| background subtraction: error on BRs | 1% | 1% |
| | | $\Delta\varepsilon_\mu/\varepsilon_\mu$ |
| $\eta$ parametrization | | 0.5% |
| | $\Delta\varepsilon_{\phi\phi}/\varepsilon_{\phi\phi}$ | $\Delta\varepsilon_{J/\psi\phi}/\varepsilon_{J/\psi\phi}$ |
| polarization in MC | 7% | 6% |
| | | $\Delta\varepsilon_{\phi\phi}/\varepsilon_{J/\psi\phi}$ |
| XFT particle dep. | | 4% |

Table 15: *The main systematic effects.*

## 10.5 Errors on Branching Ratios

We use for the BR($J/\psi \to \mu\mu$) and BR($\phi \to K^+K^-$) the the PDG values [11] thus contributing respectively 1.0% and 1.2% to the total relative uncertainty.

The PDG value of the BR($B_s^0 \to J/\psi\phi$) is, on the other end, a CDF measurement from Run I. At the time $\frac{f_s}{f_d} = 0.40 \pm 0.06$ was used, but the present value in 2008 PDG is somewhat incompatible ($\frac{f_s}{f_d} = 0.28 \pm 0.04$). We rescale the CDF I $B_s^0 \to J/\psi\phi$ BR by the ratio of the old to the current $f_d/f_s$ values to obtain:

$$\mathrm{BR}(B_s^0 \to J/\psi\phi) = (1.35 \pm 0.46) \cdot 10^{-3} \tag{21}$$

Since the latter uncertainty is large and could possibly be reduced by either CDF or Belle in a not too distant future we will single out the effect from the still limited knowledge of $B_s^0 \to J/\psi\phi$ Branching Ratio in the systematic uncertainty of our measurement.

## 10.6 Summary

In Table 15 we summarize the main systematic effects for the measurement of the BR. Summing in quadrature the evaluated systematics we derive a total relative uncertainty of 12% excluding the $B_s^0 \rightarrow J/\psi\phi$ Branching Ratio error.

# 11 Results

We studied the $B_s \rightarrow \phi\phi$ and $B_s \rightarrow J/\psi\phi$ decays using a sample of $2.9 fb^{-1}$ collected using the Two Track Trigger in CDFII since 2002 until April 2008.

The number of events obtained in the two decays channels are:

$$\begin{aligned} N_{\phi\phi} &= 295 \pm 20(\text{stat}) \pm 12(\text{syst}) \\ N_{J/\psi\phi} &= 1766 \pm 48(\text{stat}) \pm 41(\text{syst}) \end{aligned}$$

Using the formula of Eq.9, we obtain:

$$\frac{BR(B_s^0 \rightarrow \phi\phi)}{BR(B_s^0 \rightarrow J/\psi\phi)} = [174 \pm 11(stat) \pm 22(syst)] \cdot 10^{-4}$$

from which, using the Branching Ratio of $B_s \rightarrow J/\psi\phi$ [11], modified according to the updated measurements of the ratio of production cross section of $B_s$ and $B_d$ mesons, we have:

$$BR(B_s^0 \rightarrow \phi\phi) = [2.35 \pm 0.15(stat) \pm 0.29(syst) \pm 0.80(BR)] \cdot 10^{-5}$$

The last uncertainty (BR) is now the dominant contribution and arise from the error of the BR ($B_s^0 \rightarrow J/\psi\phi$) alone.

Comparing this result with that of the first publication [1], we see that there is a good agreement and a substantial improvement on the statistical uncertainty.

Another important result of this work is the evaluation of a sample of $B_s \rightarrow J/\psi\phi$ decays independent from the `DI_MUON` trigger, which is used in CDFII to study such decays. We have shown that the use of the TTT events can increase of 25 % the sample of $B_s \rightarrow J/\psi\phi$ decays.

# 12 Outlook

CDFII is expected to collect by the end of 2009 an integrated luminosity of 6-8 $fb^{-1}$ and if the data taking run will be extended to 2010, an additional 2 $fb^{-1}$ will be available. It is clear therefore that, despite the suppression that the Two Tracks Trigger has at high instantaneous luminosity, we expect to conclude the Run II with a significant increase of the data samples of these decays.

Besides the new measurement of the BR($B_s^0 \rightarrow \phi\phi$), this analysis represents as well the preparatory work and the first step towards the measurement of the polarization in the channel $B_s \rightarrow \phi\phi$. It has allowed a comprehensive understanding of the different signal components in the TTT, the background and the trigger and prescale effects.

# 13 History of Changes to This Document

- **v4.0**

  1. Add several clarification throughout to respond to question raised during pre-blessing
  2. Greatly expanded section9 on muon identification efficiency, including few bug fixes that slightly change central value and uncertainty.
  3. Change statistical uncertainty of the fitted signal yields to correct for a mistake present in **v3.0**

# References


[1] D'Auria et al., CDF Note 6937, "Search for $B_s^0 \to \phi\phi$ decays at CDF".

[2] D.Acosta et al. (CDF Collaboration),*Phys. Rev. Lett.* **95**, 031801, 2005.

[3] G. Punzi, proceeding of PHYSTAT2003, SLAC Sept 8–11,2003. "Sensitivity of searches for new signals and its optimization," eConf **C030908**, MODT002 (2003); arXiv:physics/0308063.

[4] D.Tonelli, CDF Note 9509, "A Simulation-free, Unbiased Optimization of the Selection".

[5] G. De Lorenzo, M. Rescigno, *Measurement of the polarization amplitudes in* $B \longrightarrow J/\psi K^*$ *and* $B \longrightarrow \phi K^*$ *using Two Track Trigger at CDF*, CDF Note n 8096, July 2006.

[6] A. Datta, D. London, J. Matias, M. Nagashima and A. Szynkman, *Final-state Polarization in* $B_s$ *decays*, 2006, [hep-ph/0802.0897].

[7] C.Paus, $B_S$ *Mixing Workshop*, January 31, 2005

[8] K. Anikeev, C. Paus, P. Murat, *Description of Bgenerator II*, CDF Note n.5092, August 1999.

[9] Mary Bishai,*et al.Measurement of the b-Hadron Inclusive Cross-section in CDF Run II using* $b \rightarrow J/\psi\ X$ CDF Note n.6285

[10] D. Lange, A. Ryd, *The EvtGen Event Generator Package*, CHEP proceedings 1998.

[11] Particle Data Group; Phys. Lett. **B667**, 1 (2008).

[12] Y. Gotra, J. Kraus and T. Miao, *Run II Level I Low* $p_t$ *Muon Trigger Efficiency Measurement*, CDF Note n.6162, 2003.

[13] S.Giagu, M.Rescigno, *et al.* Cdf Note 6391